The Meteoritical Society

*Meteoritics & Planetary Science* 42, Nr 4/5, 709–729 (2007)
Abstract available online at http://meteoritics.org

# Uppermost impact fallback layer in the Bosumtwi crater (Ghana): Mineralogy, geochemistry, and comparison with Ivory Coast tektites

Christian KOEBERL[1*], Franz BRANDSTÄTTER[2], Billy P. GLASS[3], Lutz HECHT[4], Dieter MADER[1], and Wolf Uwe REIMOLD[4]

[1]Department of Geological Sciences, University of Vienna, Althanstrasse 14, A-1090 Vienna, Austria
[2]Mineralogisch-Petrographische Abteilung, Natural History Museum, Burgring 7, A-1010 Vienna, Austria
[3]Department of Geology, University of Delaware, Newark, Delaware 19716, USA
[4]Mineralogy, Museum for Natural History, Humboldt University in Berlin, Invalidenstrasse 43, D-10115 Berlin, Germany
[*]Corresponding author. E-mail: christian.koeberl@univie.ac.at

*(Received 01 October 2006; revision accepted 01 January 2007)*

**Abstract**–In 2004, an International Continental Scientific Drilling Program (ICDP) drilling project at the Bosumtwi impact crater, Ghana (10.5 km in diameter, 1.07 Myr old), was performed to study the sediments that fill the lake as well as the underlying impactites. In one (LB-05) of 16 cores drilled into the lake sediments, the zone between the impact breccias and the post-impact sediments was penetrated, preserving the final, fine-grained impact fallback layer. This ~30 cm thick layer contains in the top 10 cm "accretionary" lapilli, microtektite-like glass spherules, and shocked quartz grains. Glass particles—mostly of splash form less than 1 mm size—make up the bulk of the grains (~70–78% by number) in the coarser size fraction (>125 μm) of the top of the fallback layer. About one-third of all quartz grains in the uppermost part of the layer are shocked, with planar deformation features (PDFs); almost half of these grains are highly shocked, with 3 or more sets of PDFs. K-feldspar grains also occur and some show shock deformation. The abundance of shocked quartz grains and the average shock level as indicated by the number of sets of PDFs, for both quartz and K-feldspar, decrease with depth into the layer. The well-preserved glass spherules and fragments are chemically rather homogeneous within each particle, and also show relatively small variations between the various particles. On average, the composition of the fallback spherules from core LB-5B is very similar to the composition of Ivory Coast tektites and microtektites, with the exception of CaO contents, which are about 1.5 to 2 times higher in the fallback spherules. This is a rare case in which the uppermost fallback layer and the transition to the post-impact sediments has been preserved in an impact structure; its presence indicates that the impactite sequence at Bosumtwi is complete and that Bosumtwi is a very well-preserved impact crater.

## INTRODUCTION AND GEOLOGICAL SETTING

The Bosumtwi impact structure in south-central Ghana is associated with the Ivory Coast strewn field, one of the four known tektite strewn fields (e.g., Koeberl et al. 1997). Bosumtwi is a well-preserved complex impact structure (centered at 06°30′N, 01°25′W) and is situated about 32 km southeast of Kumasi, the capital of the Ashanti region of Ghana. The crater has a distinct, steep rim with elevations of up to 300 m above present-day lake level and is almost completely filled by Lake Bosumtwi, which is 8 km in diameter. The crater is surrounded by a slight and irregular circular depression, as well as an outer ring of minor topographic highs with a diameter of about 20 km (Jones et al. 1981; Reimold et al. 1998; Wagner et al. 2001).

The Bosumtwi impact crater was excavated in lower greenschist facies metasediments (metagraywacke, quartzitic metagraywacke, metatuffs, phyllites, shales, and schists) of the 2.1–2.2 Gyr old Birimian Supergroup. Rocks to the southeast of the crater contain altered basic intrusives (Birimian metavolcanics) in addition to metasediments. Clastic Tarkwaian sediments occur further to the east and southeast, and are thought to have been formed by the erosion of Birimian rocks. A detailed review, describing all aspects of Bosumtwi, and a new geological map were recently published by Koeberl and Reimold (2005).

The Bosumtwi structure is one of the best-preserved


© The Meteoritical Society, 2007. Printed in USA.

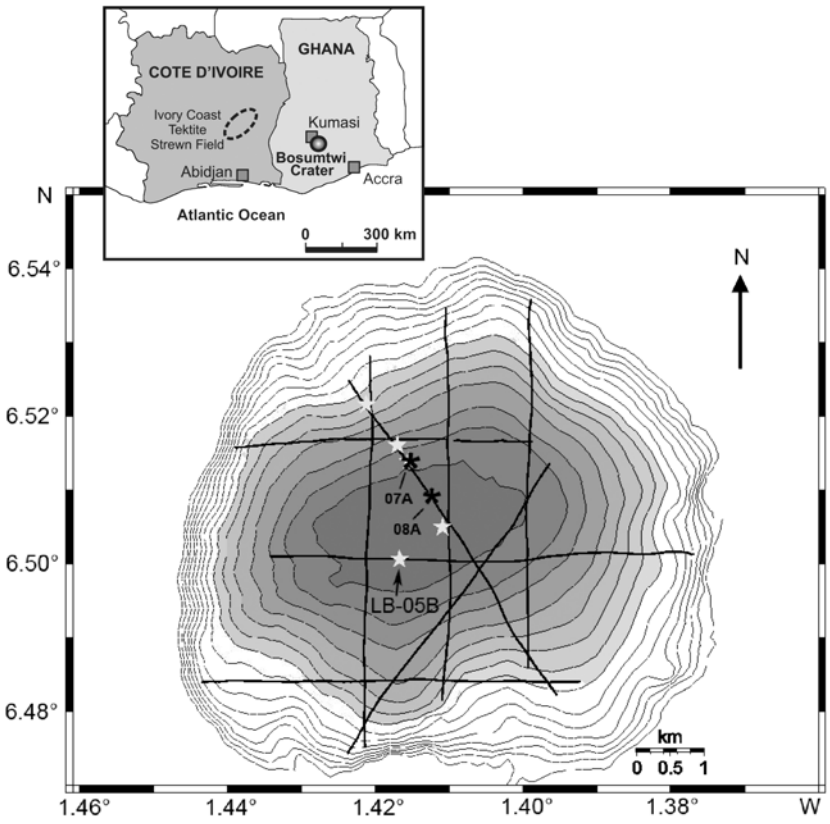


Fig. 1. A location map showing the location of borehole LB-05B, which was terminated in the uppermost fallback layer, as well as the positions of boreholes LB-07A and LB-08A, which penetrated impact breccias and fractured bedrock in the deep crater moat and the flank of the central uplift, respectively. Also shown are profiles along which seismic data were recovered (cf. Scholz et al. 2002; Karp et al. 2002) and that were used to position the drill sites.

terrestrial meteorite impact structures, with proximal ejecta in the form of suevite and other impact breccia deposited outside the crater rim, to a distance of about 1 crater radius. The crater is particularly important because of its association with the Ivory Coast tektites, which were first reported by Lacroix (1934) from an 80 km wide area in Ivory Coast (Côte d'Ivoire) territory. Microtektites were found in deep-sea cores off the coast of West Africa (Glass 1968, 1969) and related to the tektites found on land. These microtektites are up to one millimeter in size and show a variety of shapes, mostly spherical shapes, droplets, tear-drops, dumbbells, and fragments of particles of these respective shapes. The geographical distribution of microtektite-bearing deep-sea cores has been used to determine the extent of the strewn field (e.g., Glass and Zwart 1979; Glass et al. 1979, 1991), and the microtektite abundance (number/cm$^2$) and size distribution was used to accurately predict the size of the source crater located at Lake Bosumtwi (Glass and Pizzuto 1994; Glass et al. 1991).

Tektites are now known to have formed during hypervelocity impacts on Earth and to represent melts of surficial, predominantly sedimentary, precursor rocks of upper crustal composition (see, e.g., Koeberl 1994; Montanari and Koeberl 2000, and references therein). Several lines of arguments were used to conclude that Bosumtwi is most likely the source crater of the Ivory Coast tektite strewn field. These include similar chemical compositions (Schnetzler et al. 1967; Jones 1985) and similar isotopic characteristics of the tektites and rocks found at the crater (e.g., Schnetzler et al. 1966; Lippolt and Wasserburg 1966; Shaw and Wasserburg 1982; Koeberl et al. 1998), as well as the similar ages of tektites and Bosumtwi impact glasses (e.g., Gentner et al. 1964; Storzer and Wagner 1977). Precise fission track and $^{40}$Ar-$^{39}$Ar step-heating dating on both Ivory Coast tektites and Bosumtwi impact glass established a reliable age of 1.07 ± 0.05 Myr for the Bosumtwi impact event and the tektites (Koeberl et al. 1997), and the magnetostratigraphically determined age of the Ivory Coast microtektite layer also agrees with the age of the Bosumtwi crater, providing a firm basis for the link between the Bosumtwi impact and the tektite-forming event.

## CORING AT BOSUMTWI

Bosumtwi is a hydrologically closed basin, which has led to the preservation of laminated varves in the lake sediments, providing a means for high-resolution (annual) paleoclimate reconstruction in a region for which so far little data exists.

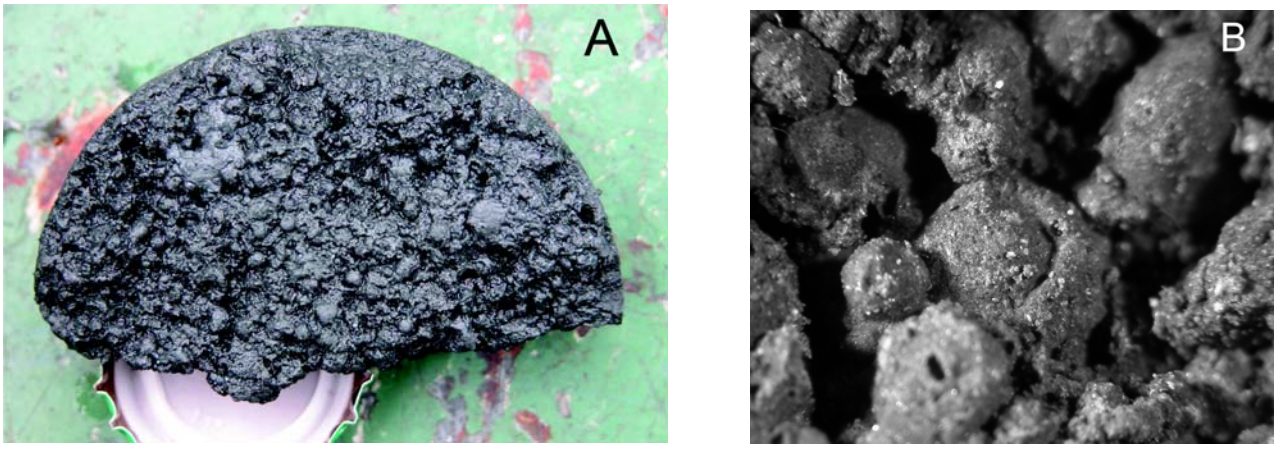


Fig. 2. a) Core segment 117A1 from the bottom of corehole LB-05B, 370.5 m below lake level, immediately after recovery of the core. Core diameter is ~5 cm. Photo courtesy M. Talbot. b) A close-up of a 4 mm wide region of the fragment shown in (a), displaying the "accretionary" spherules/lapilli. Photo courtesy J. Peck.

Together with the importance of Bosumtwi for understanding impact processes, this provided ample reason for an international and multidisciplinary drilling project, primarily financed by the International Continental Scientific Drilling Program (ICDP) (cf. Koeberl et al. 2005, 2006, 2007). The project had two main scientific goals: paleoenvironmental studies and impact studies. From July to October 2004, 16 boreholes were drilled at 6 locations within Lake Bosumtwi as part of the ICDP drilling project. The GLAD lake drilling system (specifically constructed for drilling at lakes, see www.dosecc.org; Koeberl et al. 2007) was used to core an entire lacustrine sediment fill from lake floor to bedrock. At five sites, 14 separate holes were drilled into the lake sediments; at two sites, LB-07A and LB-08A, thick sequences of impactites and fractured bedrock were recovered. In core LB-05A (see Fig. 1 for location), the complete ~1 Myr lacustrine sediment fill was recovered from the crater interior, ending in a layer about 30 cm thick with abundant spherules on top, the upper part of which appeared to be an "accretionary" lapilli-bearing sediment (Figs. 2a and 2b). This unit likely represents the final fallback ejecta at the base of the first post-impact sediment and provides an important age constraint for the overlying sedimentary sequence. The present paper describes the components of this uppermost fallback ejecta unit.

## SAMPLES AND EXPERIMENTAL METHODS

Borehole LB-05B was drilled at a depth of 74 m layer water (6.50052°N, 1.41595°W) (Fig. 1); the total depth reached was 370.56 m, and coring was done from a depth of 75.90 m to 370.56 m, for a total core recovery of 294.67 m. The core penetrated lake sediments, but at the very bottom of the core, section 117 (see Fig. 2 for a view of a section of the core), a different rock unit was reached. This unit, with some spherule-like objects, was below the bottom of the lake sediments and assumed to be the uppermost impactite layer. No sedimentary structures are recognizable in this unit; after drying, the friable material has the form of irregular fragments. The millimeter-size spherules that are prominent in Fig. 2 have an appearance similar to accretionary lapilli (see below).

Table 1. Relative abundances of the major and accessory mineral components of accretionary spherules Sp-1 to Sp-4 and a bulk rock sample of subsample 117-A1 from core LB-05B.

| | Sp-1 | Sp-2 | Sp-3 | Sp-4 | Bulk A1 |
|---|---|---|---|---|---|
| Abundant | Qz | Qz | Qz | Qz | Qz |
| | Ab | Ab | Ab | Ab | Ab |
| | Chl | Chl | Chl | Chl | Chl |
| | Ill | Ill | Ill | Ill | Ill |
| Accessory | Ap | Ap | Ap | Py | Ap |
| | Epi | Epi | Py | Ru | Epi |
| | Py | Py | Ru | Sph | Pl |
| | Ru | | | | Py |
| | | | | | Ru |
| | | | | | Sph |

Mineral identifications by electron microscopy with EDX analysis. Abbreviations: Qz = quartz; Ab = albite; Chl = chlorite; Ill = "illite," illite-hydro-muscovite; Ap = apatite; Epi = epidote; Pl = plagioclase; Py = pyrite; Ru = rutile, Sph = sphene.

The ~30 cm thick uppermost fallback ejecta unit was divided into three subunits (117A1, 117A2, and 117A3). Hereafter these subunits will be referred to as A1, A2, and A3, respectively. Sample A1 is from the uppermost part of the fallback unit (~5 cm thick), sample A2 is immediately below A1 (~10 cm), and A3 (the lowermost ~15 cm) is just below A2. Parts of the cores from these subunits were available for the present study. From those segments thin sections were prepared, and various aliquots of (mostly of subpart A1) were studied in Vienna, Berlin, and Delaware. At the University of Delaware, samples A1 and A2 were

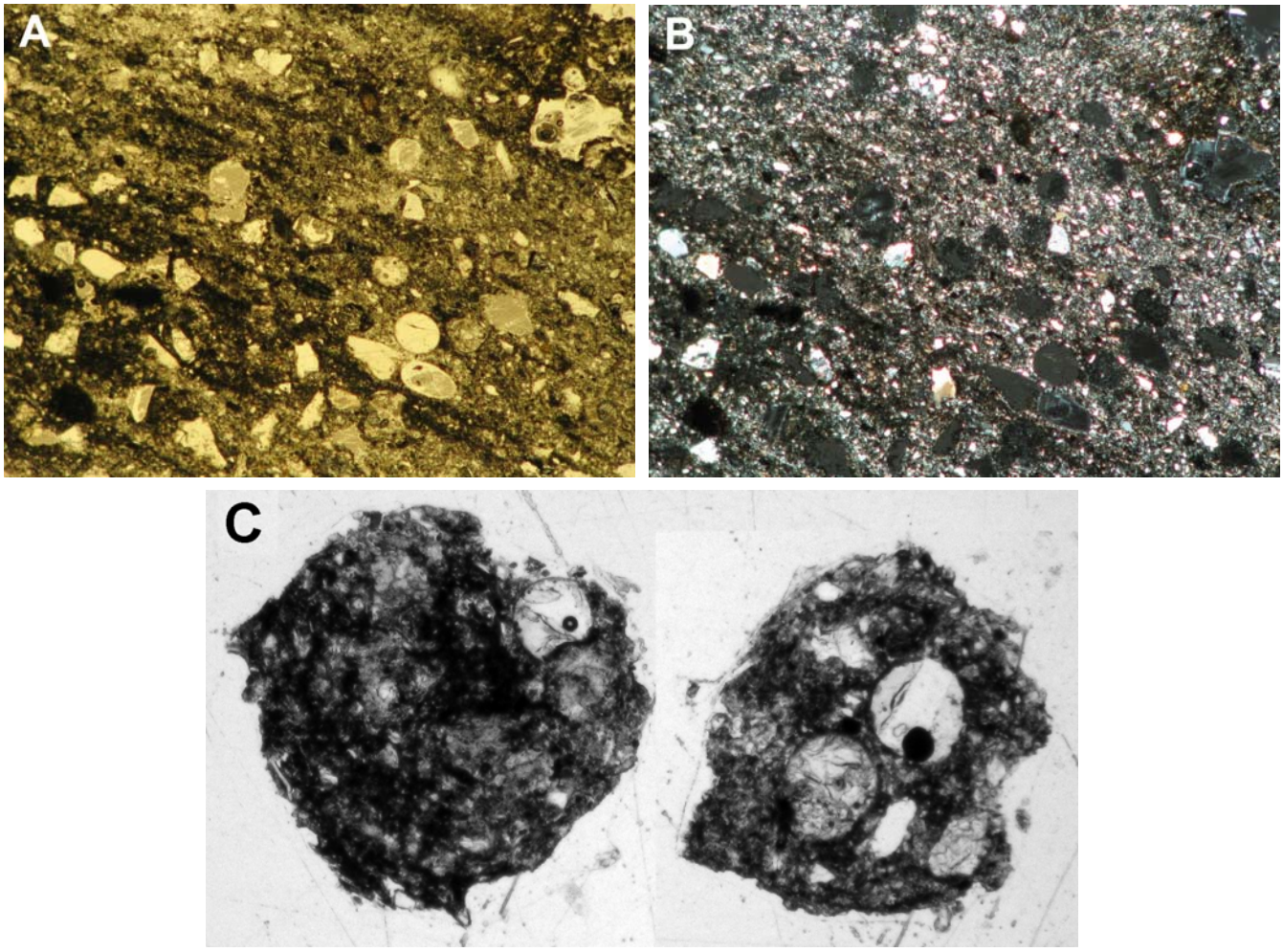


Fig. 3. a) and b) View of a 2.5 mm wide section of sample 117-A1, with numerous glassy spherules and fragments, as well as a variety of minerals, in a fine-grained matrix. a) Plane-polarized light. b) Cross-polarized light. c) Plane-polarized light microphotograph of two accretionary lapilli-like agglomerated particles (the spherule shapes that are prominent in Fig. 2), which contain some glass spherules (up to a few hundred μm in size) and fragments, as well as mineral and lithic fragments. The diameter of each lapilli is about 1 mm.

searched for glass particles and shock-metamorphosed grains. This was done by disaggregating subsamples in water using ultrasonics and sieved into five size fractions (>500, 250–500, 125–250, 63–125, <63 μm). Dilute HCl was used in an attempt to help disaggregate A1, but very little carbonate was present. A2 was disaggregated without using dilute HCl. Sample A3 could not be disaggregated and was crushed to less than 250 μm and sieved into three size fractions (125–250, 63–125, and <63 μm). The 63–125 μm size fraction of each of the three samples was separated into a heavy (specific gravity >2.96) and a light (specific gravity <2.96) fraction. The heavy mineral fractions were searched for high-pressure polymorphs (e.g., coesite, reidite). A portion of each light fraction was mounted in Piccolyte on petrographic slides and searched for shock-metamorphosed grains containing planar deformation features using a petrographic microscope.

In addition, 4 millimeter-size “spherules,” as well as a section of the core fragment ~6 mm wide, were impregnated with epoxy and prepared for polished thin sections. These were studied by optical and electron microscopy and electron microprobe analysis. Scanning and backscattered electron images were examined, and the composition and identity of minerals and glasses were determined by energy-dispersive spectrometry, using a JEOL-6400 instrument in Vienna. The composition of some glass fragments and spherules was studied by quantitative wavelength-dispersive microprobe analysis at the Natural History Museum in Vienna, using an ARL-SEMQ instrument (acceleration voltage 15 kV, beam current 20 nA) and international mineral standards. Analyses were done using a defocused beam to avoid loss of Na. Data reduction was done with standard ZAF procedures. Detection limits are at 0.01 wt% and the precision of the data is better than 5 rel%.

A further polished thin section was studied for

Table 2. Size data and percentage of glass in samples 117A1 and 117A2.

| Sample | Sample weight (g) | Size fraction (μm) | Weight (g) | Weight percent | Percent glass (by number) |
|---|---|---|---|---|---|
| 117A1[a] | 1.3368 | | | | |
| | | >500 | 0.0000 | 0.00 | n/a |
| | | 250–500 | 0.0663 | 4.96 | 78 |
| | | 125–250 | 0.0032 | 0.24 | 70 |
| | | 63–125 | 0.0362 | 2.71 | 9 |
| | | <63 | 1.2311[b] | 92.09 | |
| 117A2 | 2.5160 | | | | |
| | | >500 | 0.8241 | 32.75 | 0 |
| | | 250–500 | 0.1321 | 5.25 | 0 |
| | | 125–250 | 0.1748 | 6.95 | 0 |
| | | 63–125 | 0.1833 | 7.29 | 0.2 |
| | | <63 | 1.2017[b] | 47.76 | |

[a]Carbonate fraction removed with dilute HCl.
[b]Estimated by subtracting weights of coarser fractions from sample weight.

petrography and chemical composition of glass fragments using a JEOL-8800 electron microprobe instrument (Natural History Museum at Berlin) operating at 15 kV and 15 nA. Analyses were calibrated using Smithsonian international mineral standards. Counting times were 20 s on peak and 10 s on background. The beam size was defocused to 3 μm to avoid loss of sodium.

In addition, several of the glass spherules and fragments that were isolated at the University of Delaware from subsample A1 were analyzed for trace elements by instrumental neutron activation analysis (see Koeberl 1993 for details on method), and subsequently embedded in epoxy, polished, and analyzed by electron microprobe in Vienna, as noted above.

## RESULTS

### Mineralogical and Petrographic Observations (Bulk Sample)

The following observations are based on thin-section studies by optical and electron microscopy, on bulk samples of subsample A1. Sample A1 consists of fine- to medium-grained mineral fragments (quartz, feldspars, mica, opaques including Fe-sulfide, hematite, and Fe-Ti-oxides, chlorite/mica), as well as lithic (metagraywacke, mica schist, and granite-derived) microclasts in a phyllosilicate-rich matrix that is mostly fine-grained (generally <150 μm) and composed of clastic material (of the same minerals as in the larger fragments). Table 1 gives the relative abundances of major and accessory mineral phases as identified by electron microscopy (mineral identification aided by EDX analysis). Besides clastic components, spherical and droplet/tear-shaped glass particles, as well as irregularly shaped glass fragments, occur abundantly in this sample. The size of these particles ranges from several hundred micrometers to about 1 mm.

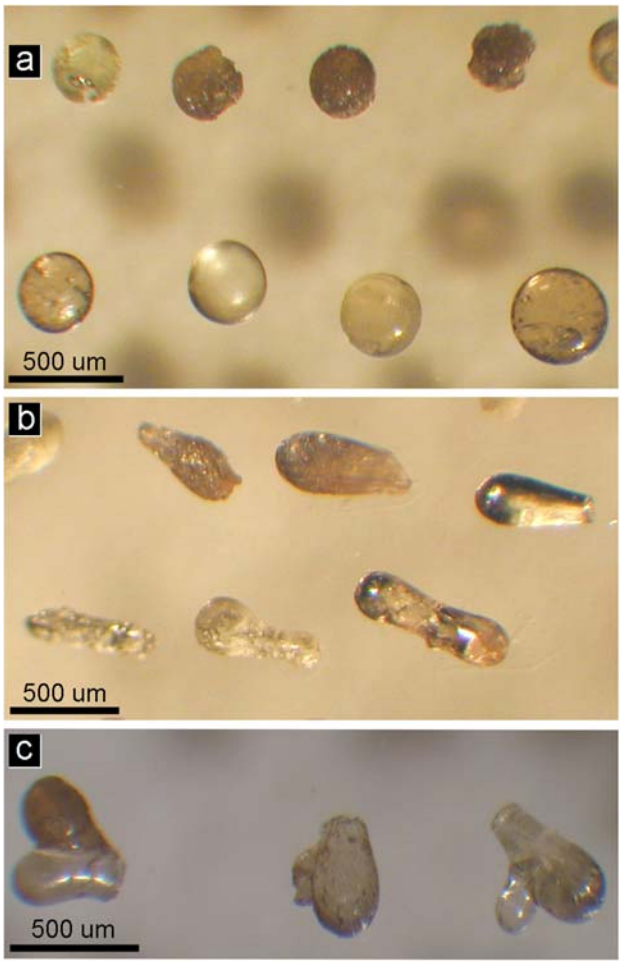


Fig. 4. Photographs of spherules recovered from sample 117A1. a) Spherical glass particles exhibiting a variety of surface textures from shiny smooth to deeply corroded. b) Examples of dumbbells and teardrops. The tails are broken off all of the teardrops; some were originally dumbbells that were broken into two teardrops. c) Three examples of teardrop pairs fused together.

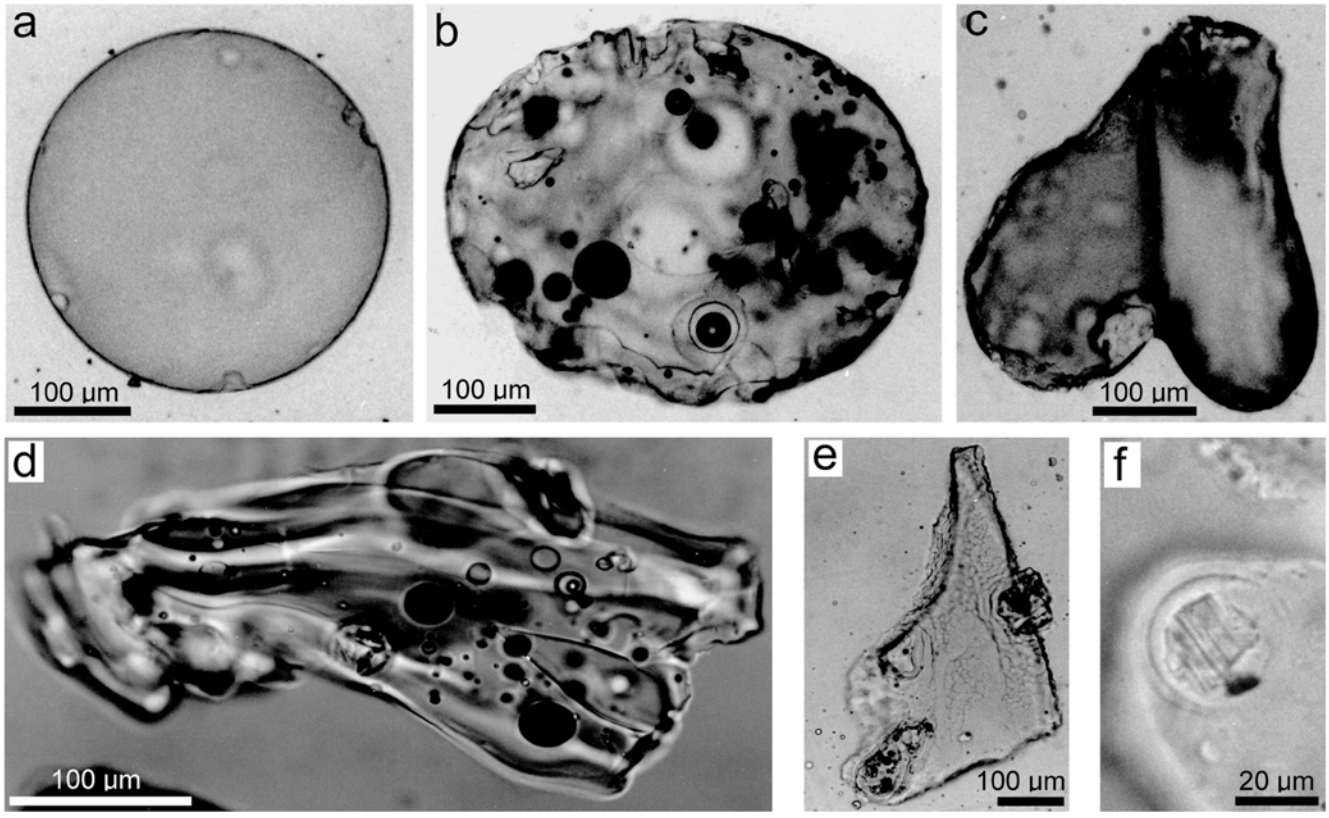


Fig. 5. Polished grain mounts of glass particles recovered from sample 117A1. a) A seemingly homogeneous sphere. b) A heterogeneous oval-shaped glass particle containing spherical vesicles and mineral inclusions. The surface is somewhat pitted. c) A pair of teardrops fused together. The teardrops have different colors and exhibit different amounts of surface pitting. d) An elongated irregular glass particle exhibiting flow structure and containing vesicles and mineral inclusions. e) An angular frosted glass fragment with two large, vesicular silica inclusions, which protrude from the surface, probably due to differential solution. f) A quartz grain, in a spherule, with two sets of planar features.

Some rounded glass bodies are aggregated with other spherules or even irregularly shaped glass particles, mineral micro-clasts, and secondary alteration products (Figs. 3a–c). Where surrounded by a thin (up to several hundred µm wide) rim of finest-grained clastic material, these accumulations resemble accretionary lapilli, as shown by the four spherules that were thin-sectioned. They are about one millimeter in diameter and contain a variety of mineral and lithic fragments, as well as smaller glass spherules and fragments (Fig. 3c). The glass particles are usually surrounded by a very thin rim of alteration phases, which may locally thicken in the form of embayments into the glass phase (possibly where shallow cracks form on the surface of the glass particles).

Tiny quartz, feldspar, or mica inclusions have been noted within such rims. Some spherules and fragments are fully or partially altered. Replacements include phyllosilicates and locally some barite, hematite, and other oxide phases. Alteration noticeably progressed from the outside inward into glass particles, most likely along fractures. With optical microscopy, two distinct glass phases could be distinguished on the basis of their respective lack of color or yellowish appearance in plane-polarized light.

Table 3. The abundance of components in the light fraction (specific gravity <2.96) of the 63–125 µm size fraction of samples 117A1 and 117A2.

| | 117A1 | | 117A2 | |
|---|---|---|---|---|
| | Number | Percent | Number | Percent |
| Rock fragments | 257 | | 295 | 49.5 |
| Quartz | 175 | 28.0 | 153 | 25.7 |
| Feldspar | 93 | 14.9 | 56 | 9.4 |
| Opaque grains | 15 | 2.4 | 33 | 5.5 |
| Other | 29 | 4.6 | 58 | 9.7 |
| Glass particles | 57 | 9.1 | 1 | 0.2 |
| | 626 | 100.0 | 596 | 100.0 |

The colorless variety is generally strongly fractured and pitted, and some of these pits seem to be aligned along possible flow structures. In contrast, the yellowish phase could be polished much better and has a very homogeneous appearance, with locally incipient crystallization being evident in the form of tiny crystallites and crystallite strings. Some shocked quartz grains were seen in the thin sections of sample 117A1s; planar fractures (PFs) are abundant, and a few grains with PDFs have been seen as well (see below).

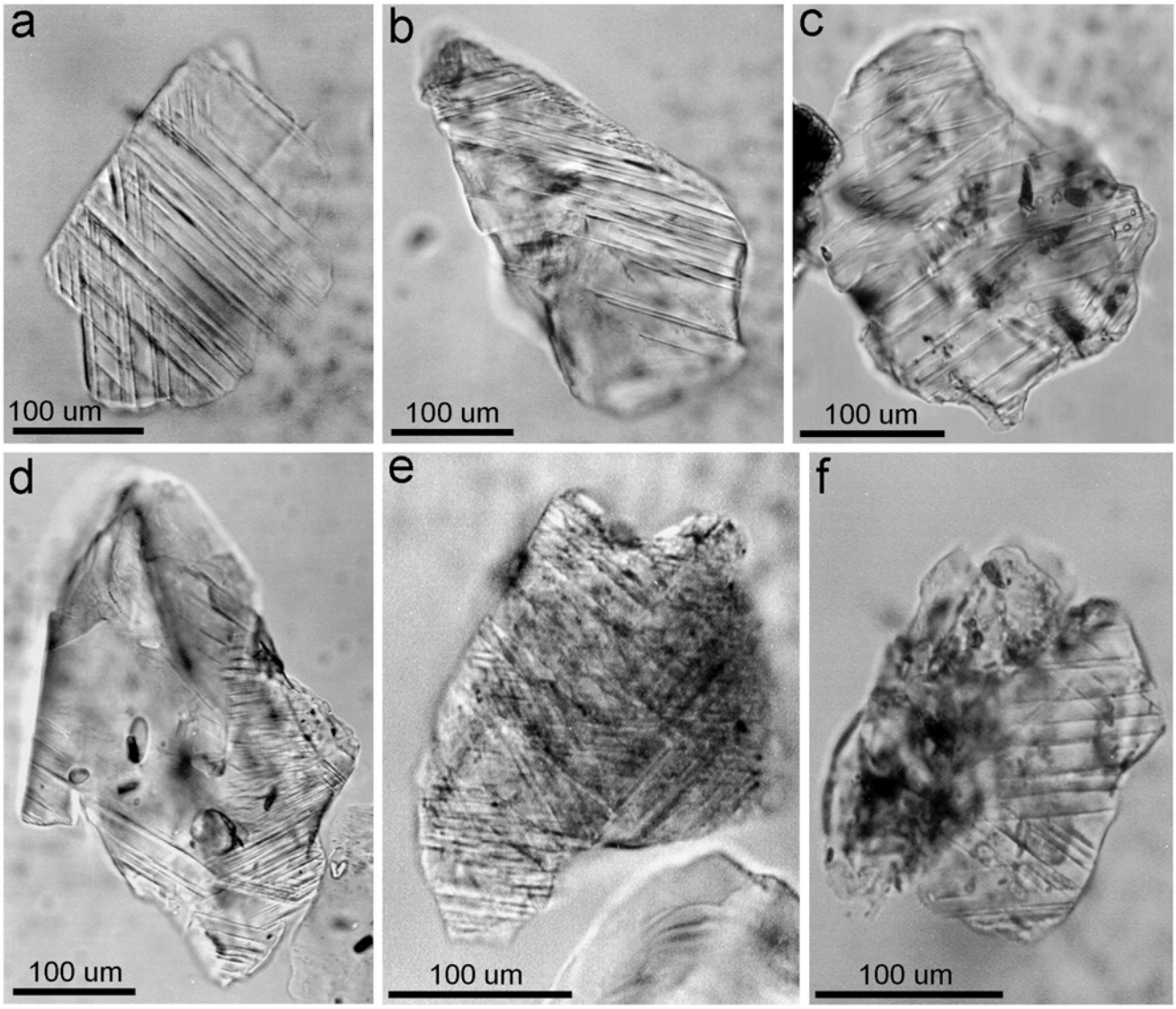


Fig. 6. Examples of grains, from sample 117A1, which exhibit planar deformation features (PDFs). a) A quartz grain containing two well-defined sets of PDFs. b) A quartz grain containing two sets of PDFs. c) A quartz grain containing 3 sets of PDFs. d) A polycrystalline grain consisting of quartz. One subgrain contains three sets of PDFs, the other grain two sets of PDFs. e) A translucent, pale yellowish brown (toasted) quartz grain containing at least 4 sets of PDFs. f) A rock fragment containing a quartz grain with two sets of PDFs.

**Grain Size and Composition**

It is clear that sample A2 is much coarser-grained than A1 (Table 2). No grains >500 μm in size were recovered from A1, but grains >500 μm make up ~33 wt% of A2. Conversely, the <63 size fraction makes up ~92 wt% of A1, but only ~48 wt% of A2. No size data were obtained for A3, as this sample could not be disaggregated. The >500 μm size fraction of A2 consists primarily of rock fragments (generally schists) and some mineral grains (mostly quartz). Quartz grains are abundant in the 63–125 μm size fraction of both A1 and A2, but extremely rare in A3. Glass particles make up the bulk of the grains (~70 to 78% by number) in the coarser size fractions (>125 μm), but only ~9% by number in the 63–125 μm size fraction of A1. On the other hand, no glass particles were recovered from the >125 μm size fraction of A2, and only a trace of glass was observed in the 63–125 μm size fraction of A2. No glass particles were observed in A3, only mineral grains and fragments.

**Glass Particles**

No glass particles were found in the >125 μm size fraction of A2 or A3; thus, the following discussion applies only to sample A1. The glass particles consist of splash forms (spheres, ovals, teardrops, dumbbells, and discs), irregular

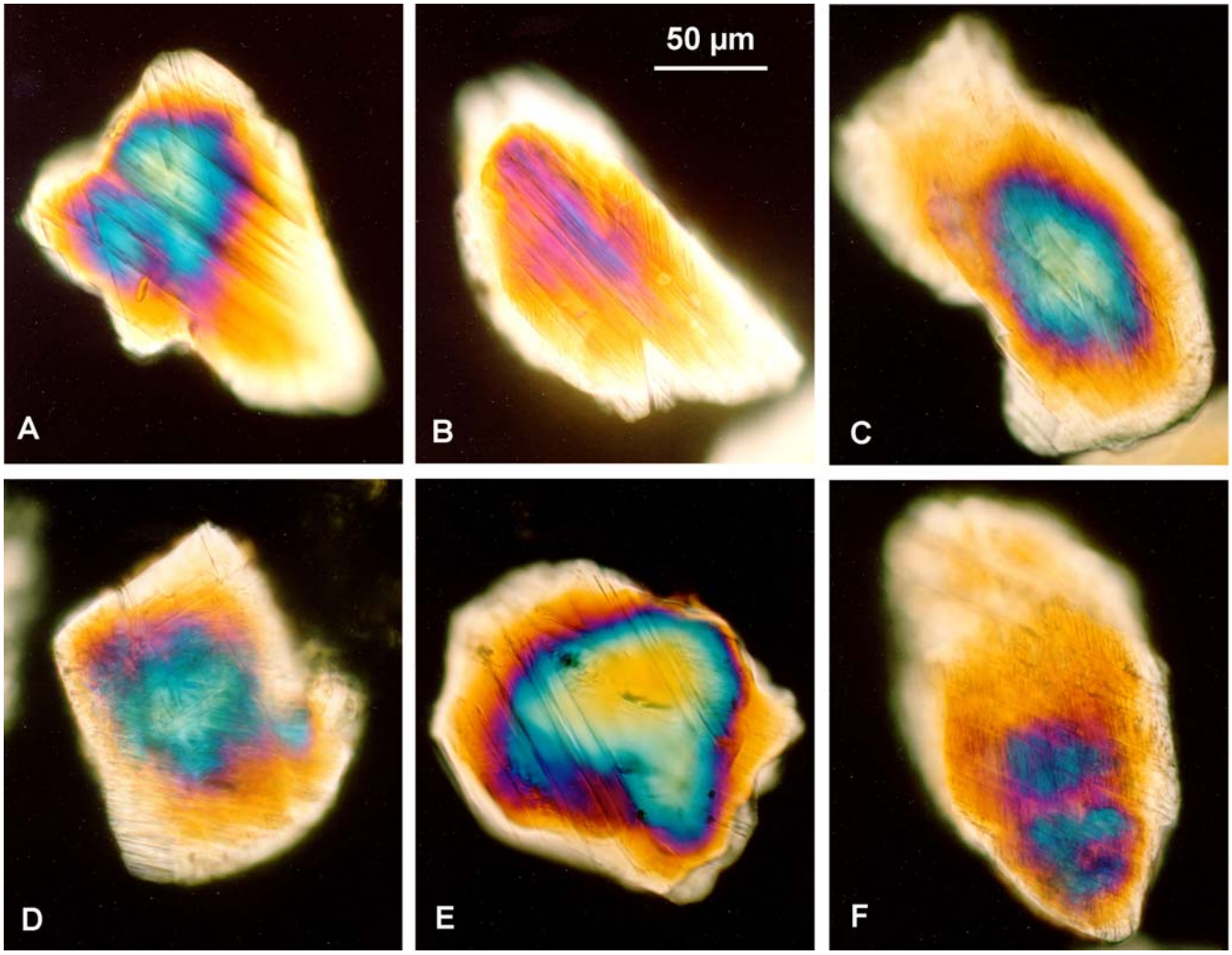


Fig. 7. Color images of single quartz grains from fallback layer 111A1, showing multiple sets of planar deformation features (PDFs).

shapes, and fragments (Figs. 4 and 5). Most glass particles are pale brown in color, but a few are dark brown. They are variably transparent to translucent. Some have some shiny smooth surfaces, but most are pitted or deeply corroded. The translucent ones generally have a finely pitted surface giving them a "frosted" appearance. Some have really exotic shapes that appear to have formed by solution of splash forms leaving silica-rich regions, which, based on their optical appearance, may be lechatelierite.

Whole splash forms make up ~38% by number of the glass particles in the 250–500 µm size fraction, but only ~9% of the glass particles in the 125–250 µm size fraction. Conversely, glass fragments make up nearly 40% by number of the 250–500 µm size fraction and 70% by number of the 125–250 µm size fraction. The remainder of the glass particles are obvious fragments of splash forms, badly etched particles that could have originally been splash forms, and irregular forms. Approximately 80% by number of the splash forms are spherical to oval in shape. The remainder are

Table 4. Percent grains containing planar deformation features.[a]

| | 117A1 | | 117A2 | |
|---|---|---|---|---|
| | Number | Percent | Number | Percent |
| Rock fragments | | | | |
| Without PDFs | 229 | 89.1 | 281 | 95.3 |
| With PDFs | 28 | 10.9 | 14 | 4.7 |
| Total | 257 | | 295 | |
| Quartz | | | | |
| Without PDFs | 124 | 70.9 | 143 | 93.5 |
| With 1 set | 14 | 8 | 5 | 3.3 |
| With 2 sets | 14 | 8 | 4 | 2.6 |
| With 3 or more sets | 23 | 13.1 | 1 | 0.7 |
| Total | 175 | | 153 | |
| Feldspar | | | | |
| Without PDFs | 72 | 77.4 | 48 | 85.7 |
| With PDFs | 21 | 22.6 | 8 | 14.3 |
| Total | 93 | | 56 | |

[a]In the light fraction (specific gravity <2.96) of the 63–125 µm size fraction.

Table 5. Major-element variation (data in wt%) along profiles across glass spherules and fragments in fallback layer subsample 117A1.

| | $SiO_2$ | $TiO_2$ | $Al_2O_3$ | MnO | FeO | MgO | CaO | $Na_2O$ | $K_2O$ | Total |
|---|---|---|---|---|---|---|---|---|---|---|
| A1-1 | 64.60 | 0.75 | 16.23 | <0.01 | 6.04 | 3.26 | 3.30 | 3.15 | 2.08 | 99.41 |
| A1-2 | 64.08 | 0.69 | 16.56 | 0.02 | 5.90 | 3.10 | 3.21 | 3.06 | 1.99 | 98.61 |
| A1-3 | 65.30 | 0.70 | 16.84 | <0.01 | 6.17 | 3.19 | 3.23 | 3.02 | 2.01 | 100.46 |
| A1-4 | 66.31 | 0.71 | 16.69 | <0.01 | 6.10 | 3.10 | 3.32 | 3.06 | 2.02 | 101.31 |
| A1-5 | 66.38 | 0.64 | 16.32 | 0.06 | 5.86 | 3.07 | 3.27 | 3.18 | 2.03 | 100.81 |
| A1-6 | 66.64 | 0.61 | 16.04 | 0.05 | 5.53 | 2.69 | 3.03 | 3.03 | 2.10 | 99.72 |
| A1-7 | 69.81 | 0.57 | 13.87 | <0.01 | 4.67 | 2.38 | 2.53 | 2.80 | 1.98 | 98.61 |
| A1-8 | 72.60 | 0.45 | 12.07 | <0.01 | 4.03 | 1.88 | 2.11 | 2.58 | 2.04 | 97.76 |
| A1-9 | 74.56 | 0.40 | 10.74 | <0.01 | 3.57 | 1.61 | 1.74 | 2.26 | 2.03 | 96.91 |
| A1-10 | 75.27 | 0.37 | 9.78 | <0.01 | 3.46 | 1.49 | 1.57 | 1.89 | 1.88 | 95.71 |
| Avg(1-7) | 66.16 | 0.67 | 16.08 | 0.04 | 5.75 | 2.97 | 3.13 | 3.04 | 2.03 | |
| A2-1 | 66.66 | 0.67 | 16.48 | 0.03 | 5.88 | 2.83 | 3.28 | 3.10 | 2.10 | 101.03 |
| A2-2 | 66.78 | 0.66 | 16.34 | 0.02 | 6.06 | 2.91 | 3.30 | 3.08 | 2.13 | 101.28 |
| A2-3 | 66.27 | 0.64 | 16.31 | 0.03 | 5.68 | 2.86 | 3.16 | 3.09 | 2.11 | 100.15 |
| A2-4 | 65.65 | 0.68 | 16.22 | 0.02 | 5.64 | 2.94 | 3.29 | 3.19 | 2.10 | 99.73 |
| A2-5 | 65.62 | 0.67 | 16.17 | 0.05 | 5.73 | 2.88 | 3.20 | 3.03 | 2.09 | 99.44 |
| A2-6 | 68.18 | 0.63 | 15.85 | 0.03 | 5.62 | 2.75 | 3.02 | 2.88 | 2.08 | 101.04 |
| A2-7 | 67.70 | 0.58 | 15.17 | <0.01 | 5.38 | 2.56 | 3.01 | 2.90 | 1.98 | 99.28 |
| A2-8 | 66.24 | 0.59 | 15.47 | 0.03 | 5.55 | 2.75 | 3.11 | 2.97 | 2.07 | 98.78 |
| A2-9 | 65.15 | 0.65 | 16.24 | <0.01 | 5.95 | 2.83 | 3.25 | 2.96 | 2.13 | 99.16 |
| A2-10 | 66.14 | 0.69 | 16.28 | <0.01 | 5.86 | 2.92 | 3.27 | 2.99 | 2.02 | 100.17 |
| Avg(1-10) | 66.44 | 0.65 | 16.05 | 0.03 | 5.74 | 2.82 | 3.19 | 3.02 | 2.08 | |
| B1-1 | 68.35 | 0.46 | 15.44 | 0.03 | 5.09 | 2.43 | 2.65 | 3.26 | 2.25 | 99.96 |
| B1-2 | 68.30 | 0.48 | 15.34 | 0.02 | 4.72 | 2.43 | 2.69 | 3.08 | 2.17 | 99.23 |
| B1-3 | 69.23 | 0.49 | 15.28 | <0.01 | 4.71 | 2.27 | 2.68 | 3.08 | 2.16 | 99.90 |
| B1-4 | 69.75 | 0.50 | 15.59 | <0.01 | 4.89 | 2.31 | 2.71 | 2.94 | 2.08 | 100.77 |
| B1-5 | 70.06 | 0.51 | 15.04 | <0.01 | 4.67 | 2.11 | 2.66 | 3.08 | 2.07 | 100.20 |
| B1-6 | 70.24 | 0.52 | 15.26 | <0.01 | 4.58 | 2.17 | 2.67 | 3.04 | 2.06 | 100.54 |
| B1-7 | 70.00 | 0.55 | 15.42 | <0.01 | 4.72 | 2.26 | 2.66 | 3.24 | 2.06 | 100.91 |
| B1-8 | 70.14 | 0.50 | 15.11 | <0.01 | 4.71 | 2.22 | 2.54 | 3.28 | 1.99 | 100.49 |
| B1-9 | 70.28 | 0.50 | 15.11 | <0.01 | 4.69 | 2.22 | 2.55 | 3.22 | 2.02 | 100.59 |
| B1-10 | 69.74 | 0.51 | 15.45 | <0.01 | 4.56 | 2.24 | 2.58 | 3.16 | 1.90 | 100.14 |
| Avg(1-10) | 69.61 | 0.50 | 15.30 | 0.03 | 4.73 | 2.27 | 2.64 | 3.14 | 2.08 | |
| B2-1 | 69.79 | 0.65 | 18.39 | <0.01 | 4.76 | 1.28 | 1.04 | 2.25 | 2.04 | 100.20 |
| B2-2 | 71.38 | 0.59 | 17.78 | <0.01 | 4.65 | 1.22 | 0.84 | 2.04 | 2.10 | 100.60 |
| B2-3 | 73.13 | 0.56 | 16.47 | <0.01 | 4.36 | 1.09 | 0.69 | 1.75 | 2.14 | 100.19 |
| B2-4 | 74.86 | 0.55 | 15.55 | <0.01 | 4.23 | 0.98 | 0.60 | 1.61 | 2.03 | 100.41 |
| B2-5 | 75.51 | 0.48 | 15.39 | <0.01 | 4.32 | 1.01 | 0.62 | 1.38 | 1.96 | 100.67 |
| B2-6 | 73.20 | 0.54 | 16.88 | <0.01 | 4.90 | 1.09 | 0.70 | 1.68 | 1.94 | 100.93 |
| B2-7 | 70.14 | 0.59 | 18.77 | <0.01 | 5.31 | 1.31 | 0.82 | 1.81 | 1.89 | 100.64 |
| B2-8 | 69.48 | 0.59 | 19.13 | <0.01 | 5.77 | 1.44 | 0.86 | 1.90 | 1.83 | 101.00 |
| B2-9 | 69.04 | 0.59 | 19.33 | <0.01 | 6.05 | 1.38 | 0.92 | 1.82 | 1.86 | 100.99 |
| B2-10 | 68.59 | 0.63 | 19.22 | <0.01 | 6.00 | 1.45 | 0.93 | 2.03 | 1.80 | 100.65 |
| Avg(1-10) | 71.51 | 0.58 | 17.69 | <0.01 | 5.04 | 1.23 | 0.80 | 1.83 | 1.96 | |
| C1-1 | 65.18 | 0.64 | 18.54 | <0.01 | 6.08 | 3.52 | 2.44 | 2.55 | 1.88 | 100.83 |
| C1-2 | 65.54 | 0.74 | 18.20 | <0.01 | 5.99 | 3.56 | 2.48 | 2.67 | 1.80 | 100.98 |
| C1-3 | 65.37 | 0.73 | 18.27 | <0.01 | 6.06 | 3.52 | 2.49 | 2.70 | 1.85 | 100.99 |
| C1-4 | 65.35 | 0.79 | 18.36 | <0.01 | 5.82 | 3.55 | 2.48 | 2.63 | 1.80 | 100.78 |
| C1-5 | 65.75 | 0.69 | 18.07 | 0.03 | 6.19 | 3.43 | 2.44 | 2.58 | 1.80 | 100.98 |
| C1-6 | 66.18 | 0.70 | 17.71 | <0.01 | 6.08 | 3.40 | 2.40 | 2.61 | 1.84 | 100.92 |
| C1-7 | 66.48 | 0.74 | 17.48 | <0.01 | 5.71 | 3.30 | 2.39 | 2.77 | 1.84 | 100.71 |
| C1-8 | 66.38 | 0.69 | 17.73 | <0.01 | 5.82 | 3.30 | 2.30 | 2.58 | 1.80 | 100.60 |
| C1-9 | 66.14 | 0.68 | 17.78 | <0.01 | 5.75 | 3.32 | 2.38 | 2.54 | 1.81 | 100.40 |

Table 5. *Continued.* Major-element variation (data in wt%) along profiles across glass spherules and fragments in fallback layer subsample 117A1.

| | $SiO_2$ | $TiO_2$ | $Al_2O_3$ | MnO | FeO | MgO | CaO | $Na_2O$ | $K_2O$ | Total |
|---|---|---|---|---|---|---|---|---|---|---|
| C1-10 | 66.25 | 0.77 | 17.58 | <0.01 | 6.04 | 3.45 | 2.38 | 2.61 | 1.75 | 100.83 |
| Avg(1-10) | 65.86 | 0.72 | 17.97 | 0.03 | 5.95 | 3.44 | 2.42 | 2.62 | 1.82 | |
| C2-1 | 55.52 | 0.52 | 15.39 | <0.01 | 5.49 | 2.54 | 1.55 | 1.91 | 1.55 | 84.47 |
| C2-2 | 64.55 | 0.60 | 17.29 | 0.03 | 5.73 | 2.51 | 1.93 | 2.01 | 1.83 | 96.48 |
| C2-3 | 66.91 | 0.64 | 17.43 | <0.01 | 5.58 | 2.52 | 1.93 | 2.11 | 1.84 | 98.96 |
| C2-4 | 68.51 | 0.65 | 16.96 | <0.01 | 5.73 | 2.59 | 1.96 | 1.98 | 1.88 | 100.26 |
| C2-5 | 69.88 | 0.64 | 17.24 | <0.01 | 5.67 | 2.45 | 1.88 | 1.98 | 1.87 | 101.61 |
| C2-6 | 69.58 | 0.69 | 17.22 | <0.01 | 5.73 | 2.49 | 1.90 | 1.86 | 1.84 | 101.31 |
| C2-7 | 69.31 | 0.65 | 16.45 | <0.01 | 5.73 | 2.46 | 1.94 | 1.80 | 1.91 | 100.25 |
| C2-8 | 70.25 | 0.63 | 16.18 | <0.01 | 5.49 | 2.29 | 1.83 | 1.86 | 1.92 | 100.45 |
| C2-9 | 68.89 | 0.62 | 16.50 | <0.01 | 5.58 | 2.41 | 1.82 | 1.94 | 1.86 | 99.62 |
| C2-10 | 67.81 | 0.67 | 17.26 | 0.02 | 5.97 | 2.56 | 2.00 | 1.86 | 1.81 | 99.96 |
| Avg(3-10) | 69.18 | 0.65 | 16.83 | 0.02 | 5.70 | 2.46 | 1.90 | 1.90 | 1.87 | |
| D1-1 | 67.27 | 0.61 | 15.73 | <0.01 | 6.11 | 2.92 | 2.40 | 2.48 | 1.70 | 99.22 |
| D1-2 | 67.64 | 0.65 | 15.75 | <0.01 | 6.00 | 3.03 | 2.29 | 2.37 | 1.79 | 99.52 |
| D1-3 | 67.61 | 0.64 | 15.88 | <0.01 | 6.08 | 2.80 | 2.39 | 2.27 | 1.73 | 99.40 |
| D1-4 | 67.65 | 0.60 | 16.26 | <0.01 | 6.15 | 3.01 | 2.40 | 2.68 | 1.66 | 100.41 |
| D1-5 | 66.54 | 0.63 | 15.89 | 0.03 | 6.06 | 2.84 | 2.46 | 2.48 | 1.74 | 98.67 |
| D1-6 | 67.24 | 0.60 | 15.76 | <0.01 | 5.86 | 2.96 | 2.38 | 2.32 | 1.74 | 98.86 |
| D1-7 | 66.52 | 0.64 | 15.96 | 0.03 | 6.00 | 2.98 | 2.34 | 2.37 | 1.71 | 98.55 |
| D1-8 | 67.17 | 0.62 | 15.70 | 0.02 | 5.93 | 2.94 | 2.44 | 2.47 | 1.67 | 98.96 |
| D1-9 | 66.53 | 0.61 | 15.80 | 0.03 | 6.00 | 2.89 | 2.46 | 2.41 | 1.67 | 98.40 |
| D1-10 | 65.99 | 0.62 | 16.05 | <0.01 | 6.02 | 3.08 | 2.47 | 2.45 | 1.73 | 98.41 |
| Avg(1-10) | 67.02 | 0.62 | 15.88 | 0.03 | 6.02 | 2.95 | 2.40 | 2.43 | 1.71 | |
| D2-1 | 66.05 | 0.74 | 17.31 | 0.03 | 6.02 | 3.26 | 2.75 | 2.35 | 1.76 | 100.27 |
| D2-2 | 66.61 | 0.70 | 17.17 | 0.02 | 6.01 | 3.23 | 2.76 | 2.41 | 1.75 | 100.66 |
| D2-3 | 66.73 | 0.74 | 17.13 | <0.01 | 6.24 | 3.23 | 2.82 | 2.14 | 1.72 | 100.75 |
| D2-4 | 66.53 | 0.66 | 17.42 | <0.01 | 6.24 | 3.09 | 2.83 | 2.39 | 1.70 | 100.86 |
| D2-5 | 66.76 | 0.76 | 17.27 | <0.01 | 5.99 | 3.18 | 2.83 | 2.30 | 1.60 | 100.69 |
| D2-6 | 66.55 | 0.72 | 17.62 | 0.03 | 5.71 | 3.19 | 2.84 | 2.24 | 1.71 | 100.61 |
| D2-7 | 66.48 | 0.71 | 17.31 | 0.05 | 5.93 | 3.11 | 2.85 | 2.20 | 1.74 | 100.38 |
| D2-8 | 66.11 | 0.73 | 17.16 | 0.03 | 6.15 | 3.20 | 2.85 | 2.29 | 1.64 | 100.16 |
| D2-9 | 66.85 | 0.66 | 17.29 | <0.01 | 5.93 | 3.22 | 2.76 | 2.16 | 1.70 | 100.57 |
| D2-10 | 65.88 | 0.65 | 16.61 | <0.01 | 6.15 | 3.09 | 2.75 | 2.20 | 1.65 | 98.98 |
| Avg(1-10) | 66.46 | 0.71 | 17.23 | 0.03 | 6.04 | 3.18 | 2.80 | 2.27 | 1.70 | |
| E1-1 | 66.69 | 0.37 | 9.09 | <0.01 | 8.35 | 1.85 | 1.81 | 3.63 | 2.81 | 94.60 |
| E1-2 | 70.16 | 0.36 | 9.11 | <0.01 | 6.77 | 1.31 | 1.07 | 3.00 | 3.15 | 94.93 |
| E1-3 | 68.65 | 0.37 | 9.90 | <0.01 | 6.37 | 1.09 | 0.85 | 2.92 | 3.29 | 93.44 |
| E2-1 | 59.68 | 0.44 | 11.03 | 0.08 | 11.78 | 3.70 | 3.73 | 4.08 | 2.29 | 96.81 |
| E2-2 | 60.30 | 0.50 | 11.35 | 0.09 | 11.68 | 3.55 | 3.69 | 3.96 | 2.29 | 97.41 |
| E2-3 | 60.45 | 0.48 | 12.04 | 0.05 | 10.28 | 3.20 | 3.30 | 3.97 | 2.47 | 96.24 |
| F1-1 | 66.68 | 0.75 | 16.48 | 0.09 | 5.80 | 3.36 | 2.73 | 2.12 | 1.74 | 99.75 |
| F1-2 | 66.38 | 0.69 | 16.27 | 0.08 | 6.00 | 3.35 | 2.77 | 2.11 | 1.69 | 99.34 |
| F1-3 | 65.74 | 0.68 | 17.15 | 0.12 | 5.76 | 3.25 | 2.86 | 2.12 | 1.59 | 99.27 |
| F1-4 | 65.88 | 0.66 | 17.48 | 0.12 | 6.11 | 3.25 | 2.91 | 2.11 | 1.60 | 100.12 |
| F1-5 | 66.75 | 0.72 | 16.79 | 0.12 | 6.13 | 3.35 | 2.96 | 2.27 | 1.70 | 100.79 |
| F1-6 | 67.34 | 0.75 | 16.77 | 0.12 | 6.05 | 3.22 | 2.85 | 2.11 | 1.69 | 100.90 |
| F1-7 | 67.12 | 0.70 | 16.74 | 0.14 | 6.06 | 3.13 | 2.90 | 2.29 | 1.69 | 100.77 |
| F1-8 | 67.03 | 0.70 | 17.04 | 0.14 | 5.72 | 3.02 | 2.87 | 2.22 | 1.76 | 100.50 |
| F1-9 | 67.22 | 0.69 | 17.14 | 0.12 | 5.98 | 3.20 | 3.04 | 2.21 | 1.66 | 101.26 |
| F1-10 | 67.01 | 0.67 | 17.33 | 0.17 | 6.28 | 3.22 | 3.10 | 2.30 | 1.70 | 101.78 |
| Avg(1-10) | 66.72 | 0.70 | 16.92 | 0.12 | 5.99 | 3.24 | 2.90 | 2.19 | 1.68 | |
| F2-1 | 65.14 | 0.68 | 16.54 | 0.18 | 6.17 | 3.22 | 3.26 | 3.20 | 1.98 | 100.37 |
| F2-2 | 65.46 | 0.67 | 16.61 | 0.20 | 6.02 | 3.40 | 3.37 | 3.02 | 1.89 | 100.64 |

Table 5. *Continued.* Major-element variation (data in wt%) along profiles across glass spherules and fragments in fallback layer subsample 117A1.

| | $SiO_2$ | $TiO_2$ | $Al_2O_3$ | MnO | FeO | MgO | CaO | $Na_2O$ | $K_2O$ | Total |
|---|---|---|---|---|---|---|---|---|---|---|
| F2-3 | 65.74 | 0.70 | 16.25 | 0.14 | 5.93 | 3.46 | 3.32 | 3.07 | 1.92 | 100.53 |
| F2-4 | 65.46 | 0.64 | 16.81 | 0.11 | 5.93 | 3.39 | 3.42 | 3.17 | 1.99 | 100.92 |
| F2-5 | 65.27 | 0.68 | 16.59 | 0.20 | 5.95 | 3.25 | 3.31 | 3.16 | 2.02 | 100.43 |
| F2-6 | 66.11 | 0.68 | 16.13 | 0.15 | 5.89 | 3.10 | 3.26 | 3.15 | 1.96 | 100.43 |
| F2-7 | 66.10 | 0.62 | 16.45 | 0.15 | 5.91 | 3.19 | 3.14 | 3.09 | 1.96 | 100.61 |
| F2-8 | 66.17 | 0.69 | 16.30 | 0.14 | 6.10 | 3.21 | 3.23 | 2.86 | 2.03 | 100.73 |
| F2-9 | 66.14 | 0.70 | 16.45 | 0.09 | 5.72 | 3.21 | 3.19 | 2.89 | 2.03 | 100.42 |
| F2-10 | 65.86 | 0.66 | 16.46 | 0.18 | 5.84 | 3.17 | 3.11 | 2.93 | 2.01 | 100.22 |
| Avg(1-10) | 65.75 | 0.67 | 16.46 | 0.15 | 5.95 | 3.26 | 3.26 | 3.05 | 1.98 | |
| F3-1 | 65.99 | 0.59 | 16.57 | 0.12 | 5.74 | 2.92 | 2.32 | 2.68 | 2.05 | 98.98 |
| F3-2 | 65.81 | 0.68 | 16.75 | 0.08 | 5.91 | 3.08 | 2.38 | 2.47 | 2.08 | 99.24 |
| F3-3 | 67.13 | 0.61 | 16.44 | 0.11 | 5.87 | 2.92 | 2.32 | 2.45 | 2.05 | 99.90 |
| F3-4 | 66.35 | 0.58 | 15.83 | 0.08 | 5.78 | 2.95 | 2.25 | 2.33 | 1.96 | 98.11 |
| F3-5 | 66.05 | 0.63 | 16.14 | 0.15 | 5.95 | 3.03 | 2.36 | 2.43 | 1.94 | 98.68 |
| Avg(1-5) | 66.27 | 0.62 | 16.35 | 0.11 | 5.85 | 2.98 | 2.33 | 2.47 | 2.02 | |
| G-1 | 68.04 | 0.74 | 17.63 | 0.10 | 5.82 | 2.86 | 2.73 | 2.41 | 1.90 | 102.22 |
| G-2 | 67.20 | 0.66 | 17.02 | 0.05 | 5.59 | 3.04 | 2.57 | 2.62 | 1.85 | 100.61 |
| G-3 | 67.83 | 0.71 | 17.25 | 0.03 | 5.56 | 2.81 | 2.79 | 2.24 | 1.85 | 101.06 |
| H-1 | 68.06 | 0.68 | 17.38 | 0.09 | 5.42 | 2.61 | 2.76 | 2.39 | 1.83 | 101.22 |
| H-2 | 67.82 | 0.69 | 17.31 | 0.03 | 5.41 | 2.14 | 2.74 | 2.18 | 1.86 | 100.19 |
| H-3 | 67.11 | 0.62 | 16.96 | 0.05 | 6.11 | 2.90 | 2.72 | 2.31 | 1.78 | 100.56 |
| I1-1 | 69.55 | 0.65 | 15.82 | 0.00 | 5.44 | 2.10 | 2.35 | 2.18 | 2.13 | 100.23 |
| I1-2 | 70.04 | 0.66 | 15.97 | 0.06 | 5.23 | 2.50 | 2.30 | 2.28 | 2.05 | 101.10 |
| I2-1 | 67.16 | 0.53 | 18.39 | 0.15 | 5.70 | 2.01 | 2.28 | 2.78 | 2.35 | 101.35 |
| I2-2 | 67.65 | 0.58 | 18.04 | 0.08 | 5.79 | 2.03 | 2.23 | 2.68 | 2.35 | 101.42 |
| I2-3 | 69.59 | 0.44 | 14.74 | 0.06 | 4.31 | 1.78 | 1.53 | 1.96 | 2.40 | 96.81 |
| I3-1 | 66.15 | 0.71 | 18.36 | 0.07 | 5.68 | 3.00 | 2.83 | 1.99 | 1.52 | 100.32 |
| I3-2 | 67.28 | 0.67 | 18.92 | 0.11 | 5.76 | 2.76 | 2.80 | 2.13 | 1.61 | 102.05 |
| I3-3 | 66.88 | 0.65 | 18.55 | 0.04 | 5.66 | 2.95 | 2.68 | 1.93 | 1.61 | 100.95 |
| I4-1 | 66.41 | 0.79 | 19.47 | 0.03 | 4.42 | 3.10 | 2.56 | 2.25 | 1.68 | 100.71 |
| I4-2 | 66.62 | 0.71 | 19.61 | 0.07 | 4.29 | 2.65 | 2.65 | 2.39 | 1.74 | 100.73 |
| I4-3 | 66.50 | 0.72 | 20.04 | 0.00 | 4.59 | 3.19 | 2.73 | 2.31 | 1.62 | 101.71 |
| I4-4 | 66.38 | 0.72 | 19.66 | 0.06 | 4.39 | 3.14 | 2.92 | 2.45 | 1.73 | 101.45 |

All data by electron microprobe analysis (Vienna). See Figs. 9a–f for profile locations.
"Avg" followed by numbers indicates the average compositions calculated for the respective glass spherules or fragments from data for unaltered parts of the various profiles (the numbers indicate which of the data points were used for the averaging).
All data (G to I) by electron microprobe analysis (Berlin). See Fig. 10 for analyses locations.

teardrop, dumbbell, and disc shapes, in decreasing order of abundance. Most of the teardrops have broken tails (Fig. 4); some originally could have been dumbbells that broke in the middle to form two teardrops. Several examples of fused pairs of side-by-side teardrops were recovered (Fig. 4). The largest sphere was an oblate sphere with a diameter of ~480 μm. The largest teardrop was 770 μm long.

The splash forms and angular fragments of glass range from homogeneous without any inclusions or vesicles to highly vesicular and containing numerous mineral inclusions and lechatelierite particles (Fig. 5). The mineral inclusions appear to be quartz, and one quartz grain appears to have two sets of planar deformation features (PDFs) (Fig. 5).

**Shocked Minerals**

The 63–125 μm size fractions of A1 and A2 were searched for quartz grains exhibiting PDFs. Approximately 600 grains from each sample were counted. Both samples contain a high percentage of rock and mineral fragments (or fine-grained ejecta that were not entirely disaggregated) (Table 3). Quartz and K-feldspar make up the bulk of the remainder of each sample. Both A1 and A2 contain rock and mineral grains exhibiting PDFs, but grains exhibiting PDFs are more abundant in A1 (Table 3; Figs. 6 and 7). Approximately 29 and 7% by number of the quartz grains in A1 and A2, respectively, contain PDFs. In A1, 45% by

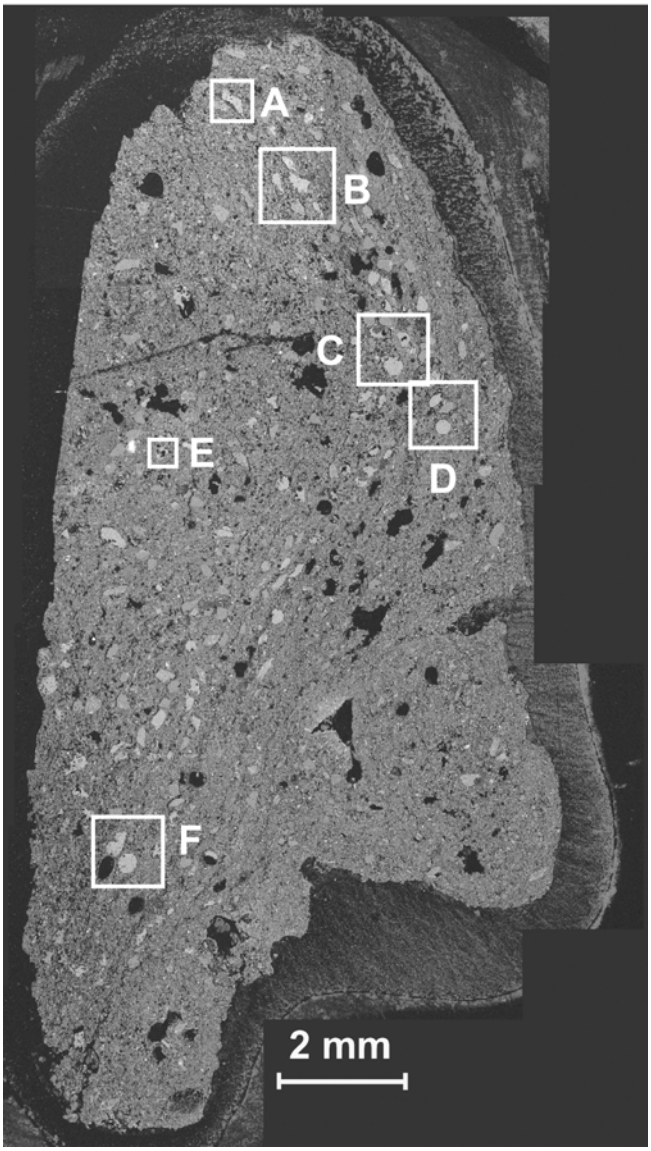


Fig. 8. An overview image of large polished thin section of a bulk fragment from fallback layer sample 117A1. The image is a mosaic of backscattered electron images and indicates the locations of the areas shown in Fig. 9, where glass fragments and spherules were analyzed by electron microprobe.

number of the quartz grains with PDFs have 3 or more sets, whereas in A2 only 10% by number of the quartz grains with PDFs have 3 or more sets (Table 4), indicating average shock pressures for these grains in excess of ~20 GPa (e.g., French 1998; Huffman and Reimold 1996). A1 also has a higher percentage of K-feldspar grains with PDFs than A2 (~23 and 14% by number, respectively). Some of the rock fragments (or polymineralic grains) in A1 and A2 contain quartz grains with PDFs (~11 and 5% by number, respectively). A preliminary search of the 63–125 μm size fraction of A3 indicates that it contains little, if any, quartz grains; no grains containing PDFs were observed.

X-ray diffraction (XRD) patterns were obtained for several white opaque grains from A1, which were thought to be shocked quartz grains that might contain coesite and/or stishovite. No coesite or stishovite lines were observed in any of the XRD patterns (in contrast to findings of coesite in fallout ejecta deposits around Bosumtwi) (Littler et al. 1961). A search was made for shocked zircons in the heavy mineral fractions of samples A1, A2, and A3. Only one zircon grain was recovered and it exhibited no signs of shock metamorphism.

## Chemical Composition of Glass

Electron microprobe analyses were made of several of the glass fragments and glass spherules. In some of the spherules and fragments, compositions are somewhat

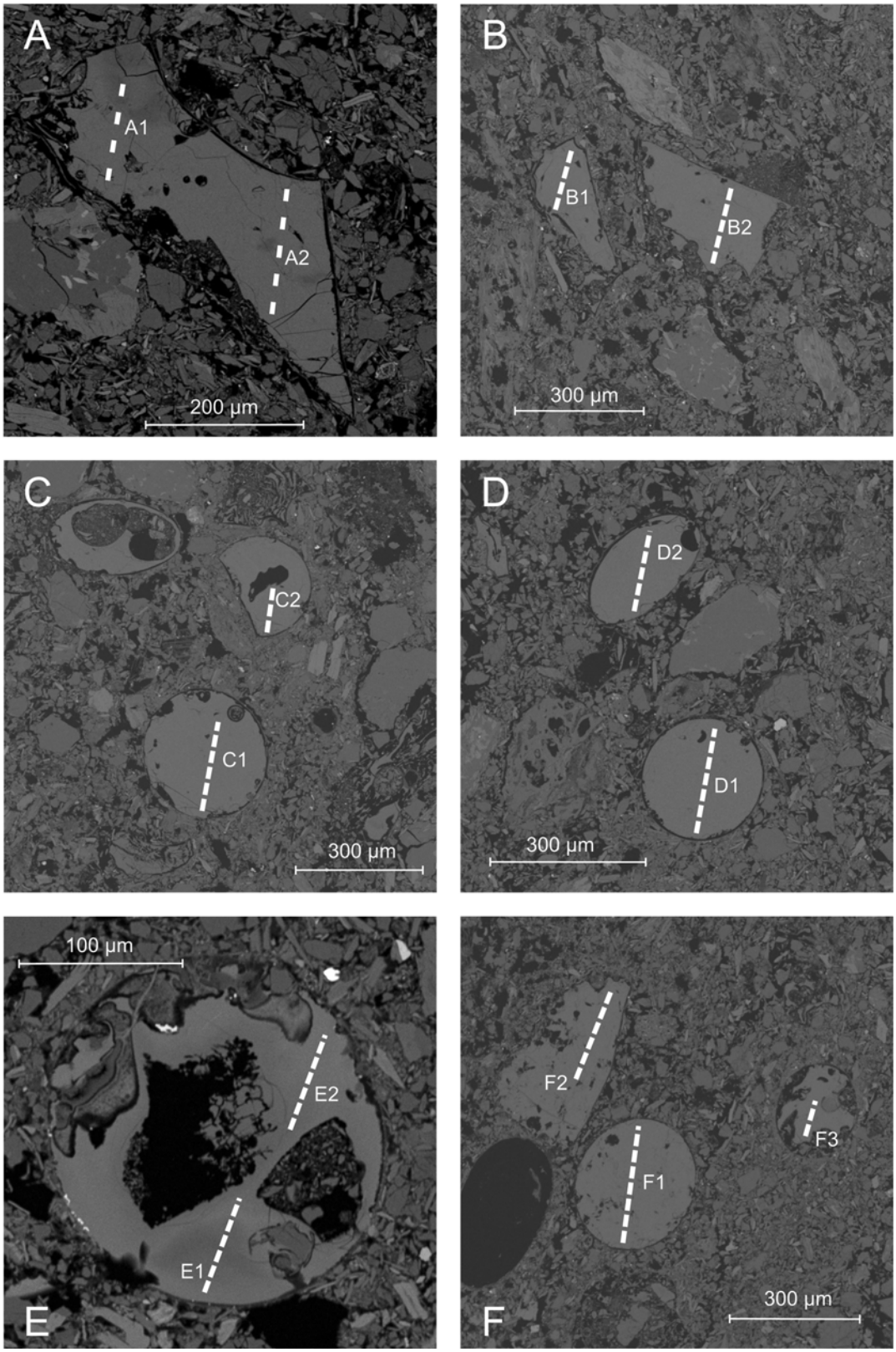


Fig. 9. a–f) Backscattered electron images of areas within a larger thin section (see Fig. 8). The positions of electron microprobe profiles are indicated by white dashed lines. The abbreviations (A1, A2, etc.) refer to the data given in Table 5. Within each profile, the analyses started at the bottom of the line and ended at the top of the line; analyses (for number of analyses in each profile see Table 4) were regularly spaced along the length of the profile.

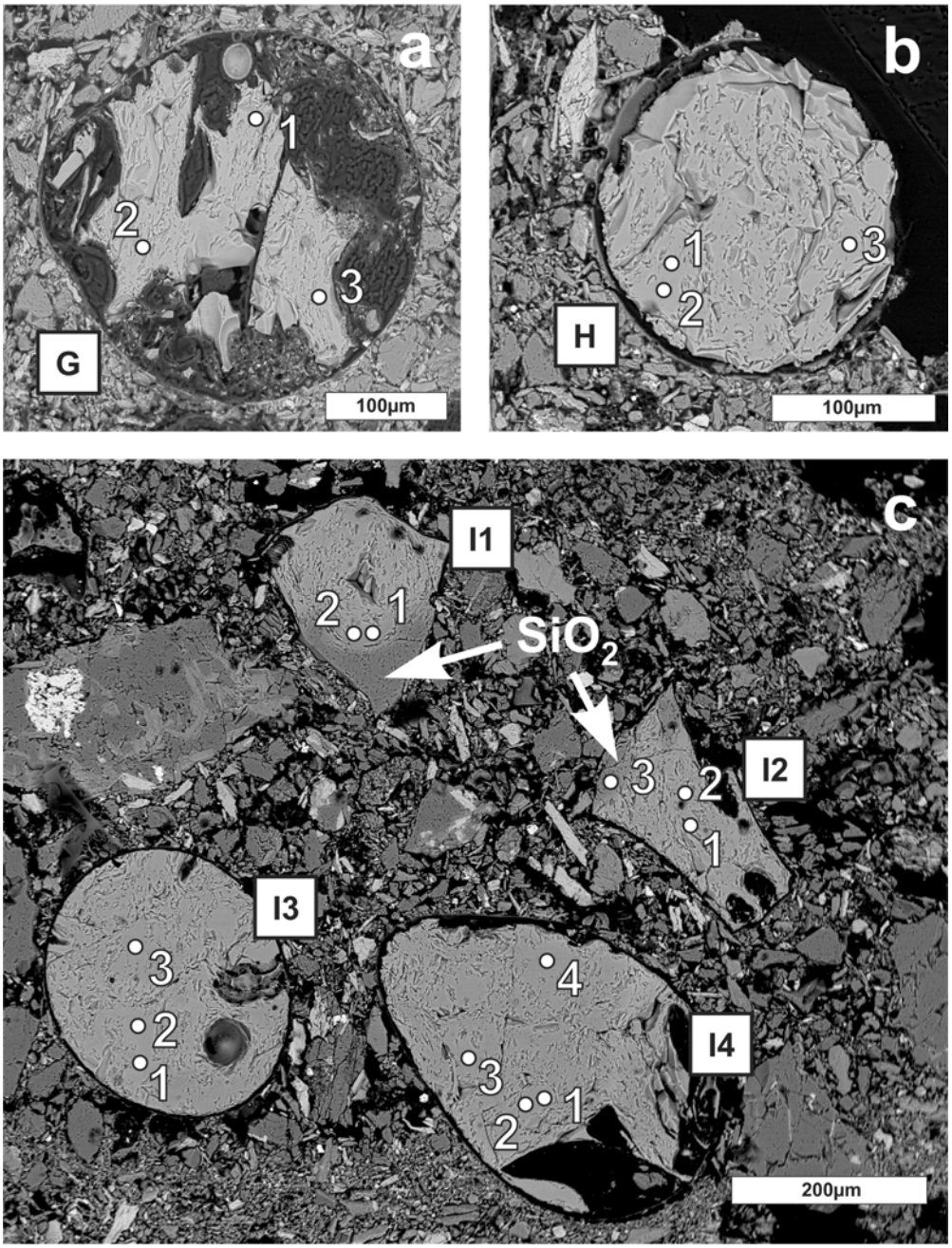


Fig. 10. Backscattered electron images of areas within a thin section of sample 117A1 that was studied by electron microprobe in Berlin. The positions of electron microprobe analyses (G to I) refer to data listed in Table 5.

variable. This appears to be due to incompletely digested minerals grains, as some zones are almost pure silica. Most other glass fragments and spherules (and other splash forms) are of rather uniform composition. Table 5 gives detailed data on the variation of compositions within 13 different glass fragments and spherules, as well as the average compositions for each of the particles. The locations of the areas in which the glasses were analyzed in the thin sections are shown in a mosaic of backscattered electron images in Fig. 8. Major element compositions were also measured by electron microprobe along profiles across the glasses; in most cases 10 points were measured per profile. Figure 9 shows the exact locations of the profiles measured in Vienna on the various glass fragments and spherules, and Fig. 10 shows the locations on another thin section analyzed in Berlin. In most cases the data for the individual analysis points showed very little radial change in composition over tens to hundreds of micrometers. Figure 11 gives two examples of the variations of selected major element contents along two of the profiles, confirming the absence of any significant heterogeneities.

In most cases totals for these analyses are close to 100 wt%, indicating that the glasses are not significantly hydrated (altered). Variations of the average compositions of 11 of the 13 glass particles (excluding the altered ones of profiles E1 and E2) are limited and range from about 30 relative% (rel%) for Ca and Mg to 5 rel%, and less for Si, Al, and Fe. In a few cases, the backscattered electron images show slight variations in contrast, indicating alteration or original heterogeneities. One such case is shown in Fig. 9e (data in Table 5), where low totals in parts of the profile indicate incipient alteration of the glass to phyllosilicate minerals. Where such alteration occurs, the spherical outline of the glasses are retained (e.g., Fig. 10a) and the bulk of the glass remaining inside such a spherule has a similar composition to that of unaltered glass spherules. For example, electron microprobe measurements made in Berlin of the glass within the spherule shown in Fig. 10a give values (Table 5, points G1–G3) that are very similar to those for other unaltered glass given in Table 5. Data obtained in Berlin and in Vienna agree within the errors of analysis.

The data for the glass spherules and fragments analyzed for both major- and trace-element contents are given in Table 6, together with comparison values for Ivory Coast tektites and microtektites. Despite the more limited precision of the current trace-element data compared to the earlier microtektite data, a general similarity is evident. The contents of refractory elements, such as Sc, Rb, the rare earth elements (REEs), Hf, and Th are very similar. The siderophile elements show more variation in abundance; the Co contents of all of the 117A1 glass spherules is somewhat higher than those of the microtektites, and a few of the samples also have relatively high Cr and Ni contents.

## DISCUSSION

The uppermost fallback ejecta unit is normally size graded with the proportion of material with larger grain size increasing with depth. The highest glass content (including spherules) and highest degree of shock metamorphism (as indicated by the proportion of grains with multiple sets of PDFs) occurs at the very top. Both glass content and degree of shock metamorphism decrease abruptly with depth.

The Ivory Coast microtektites, which are believed to be derived from the Bosumtwi crater, are generally darker and more greenish in color than the spherules found in the uppermost fallback ejecta layer at Bosumtwi crater. The shapes are similar, but the Ivory Coast microtektites have a greater range in size and a different size distribution than the Bosumtwi crater spherules. The largest spherical Ivory Coast microtektite is ~500 μm in diameter and the abundance increases with decreasing size down to at least 60 μm. The largest Bosumtwi spherule is about ~480 μm, but most of the spherical Bosumtwi spherules are about 200 μm in diameter and none are smaller that 160 μm in diameter. In contrast to the Bosumtwi spherules, the Ivory Coast microtektites are devoid of mineral inclusions and are generally less vesicular (e.g., Glass 1968, 1969; Glass and Zwart 1979).

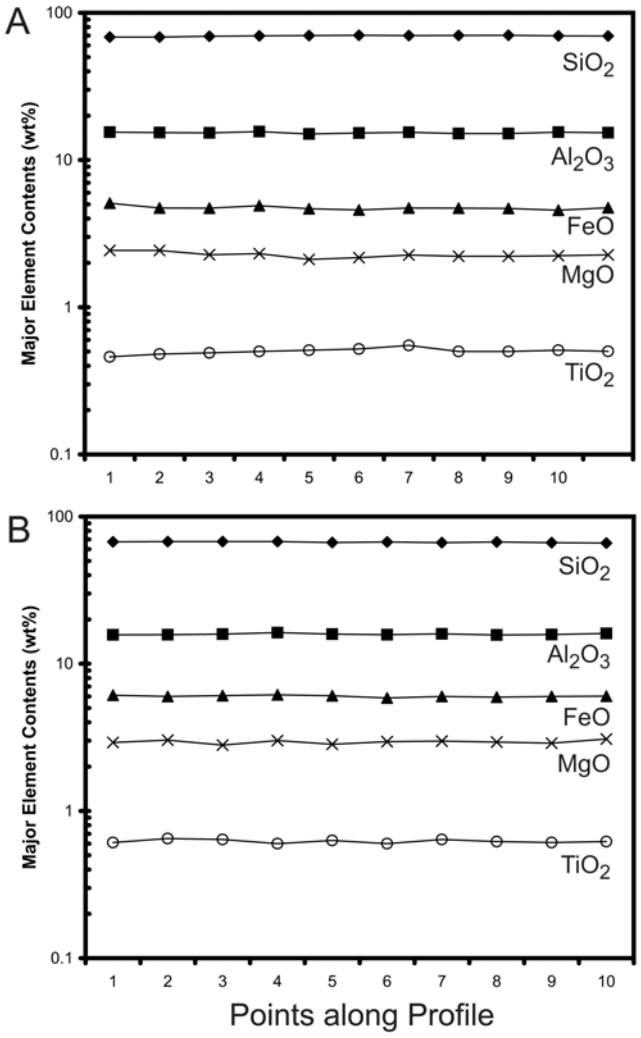


Fig. 11. Profiles of elemental compositions across (a) glass fragment B1 and (b) glass spherule D1, showing a fairly homogenous composition in both cases.

The greener color of the Ivory Coast microtektites might be the result of the higher temperature of formation of the microtektites compared with the Bosumtwi spherules, which caused reduction of the iron resulting in the greenish color of the glass. A higher temperature of formation of the microtektites is supported also by the lack of mineral inclusions and generally fewer vesicles in the microtektites, compared with the Bosumtwi spherules.

A comparison of the compositions of the glass fragments and spherules in sample LB-05B-117-A1 with those of Ivory Coast tektites and microtektites shows relative similarity (Figs. 12 and 13). Detailed data are given in Tables 6 and 7. The contents of $SiO_2$, $Al_2O_3$, FeO, and $K_2O$ in the fallback glasses agree very well with both tektite and microtektite data

Table 6. The compositions of 15 glass spherules and fragments from sample 117A1. Major elements (in wt%) by electron microprobe; trace elements (in ppm) by neutron activation analysis.

| Sample | #1 | #3 | #4 | #6 | #7 | #8 | #9 | #10 | #12 | #15 | #16 | #17 | #18 | #19 | #20 | Tektites avg. | Microtektites |
|---|---|---|---|---|---|---|---|---|---|---|---|---|---|---|---|---|---|
| Weight (µg) | 29.6 | 67.6 | 42.0 | 22.1 | 33.0 | 33.8 | 56.9 | 35.5 | 52.4 | 51.0 | 34.4 | 35.1 | 45.0 | 43.6 | 54.4 | | |
| $SiO_2$ | 60.00 | 70.13 | 67.50 | 67.44 | 66.79 | 68.11 | 68.86 | 66.32 | 67.84 | 67.45 | 67.78 | 67.70 | 67.89 | 67.59 | 65.09 | 67.58 | 67.37 |
| $TiO_2$ | 0.98 | 0.53 | 0.69 | 0.72 | 0.68 | 0.61 | 0.53 | 0.63 | 0.65 | 0.59 | 0.63 | 0.63 | 0.52 | 0.55 | 0.68 | 0.56 | 0.59 |
| $Al_2O_3$ | 12.19 | 15.41 | 15.67 | 16.38 | 16.89 | 13.28 | 13.86 | 14.94 | 15.60 | 15.81 | 15.33 | 16.58 | 15.58 | 13.98 | 17.98 | 16.74 | 17.07 |
| MnO | 0.09 | 0.02 | 0.05 | 0.05 | 0.07 | 0.09 | 0.08 | 0.07 | 0.05 | 0.08 | 0.08 | 0.08 | 0.07 | 0.07 | 0.06 | 0.06 | 0.07 |
| FeO | 8.26 | 4.59 | 6.24 | 5.92 | 5.99 | 5.97 | 5.88 | 6.28 | 6.15 | 6.17 | 5.64 | 5.49 | 5.32 | 5.87 | 5.87 | 6.16 | 6.40 |
| MgO | 8.19 | 2.11 | 3.54 | 3.15 | 3.00 | 3.19 | 2.76 | 3.20 | 3.02 | 3.13 | 3.27 | 3.23 | 2.34 | 2.93 | 2.83 | 3.46 | 3.70 |
| CaO | 5.41 | 2.72 | 2.90 | 2.68 | 2.56 | 2.59 | 2.09 | 2.99 | 2.51 | 2.59 | 3.44 | 3.25 | 2.21 | 2.86 | 2.34 | 1.38 | 1.22 |
| $Na_2O$ | 2.67 | 3.49 | 2.32 | 1.59 | 2.59 | 2.13 | 2.76 | 2.88 | 2.37 | 2.52 | 2.14 | 2.07 | 2.88 | 2.99 | 2.87 | 1.90 | 1.63 |
| $K_2O$ | 1.35 | 1.82 | 1.64 | 1.68 | 1.99 | 1.47 | 2.26 | 2.04 | 2.00 | 1.85 | 1.54 | 1.66 | 2.23 | 2.06 | 2.09 | 1.95 | 1.86 |
| Total | 99.14 | 100.83 | 100.54 | 99.60 | 100.56 | 97.43 | 99.07 | 99.34 | 100.19 | 100.18 | 99.84 | 100.69 | 99.05 | 98.90 | 99.80 | 99.79 | 99.91 |
| Sc | 25.9 | 18.7 | 17.6 | 14.8 | 15.2 | 18.9 | 16.1 | 16.6 | 17.1 | 18.3 | 19.8 | 16.6 | 15.7 | 17.1 | 17.7 | 14.7 | 17.9 |
| Cr | 285 | 83 | 212 | 99 | 135 | 156 | 136 | 159 | 158 | 125 | 140 | 160 | 107 | 163 | 147 | 244 | 293 |
| Co | 71.4 | 30.8 | 37.5 | 47.5 | 40.5 | 44.1 | 32.6 | 41.9 | 46.5 | 52.1 | 58.9 | 56.7 | 53.3 | 56.3 | 53.5 | 26.7 | 32.7 |
| Ni | 150 | <1000 | <700 | 650 | <1000 | <1000 | 510 | 520 | <1000 | 170 | 430 | <1000 | 180 | <700 | <600 | 157 | 224 |
| Rb | 47 | 96 | <150 | <100 | <100 | 30 | 20 | 140 | 160 | <100 | 110 | 58 | 58 | <100 | <100 | 66 | 67 |
| Zr | 180 | <600 | <1000 | <200 | <500 | <500 | 160 | <600 | <1000 | 200 | 580 | <400 | 470 | 280 | <1000 | 134 | 215 |
| Sb | <1 | 0.16 | <1 | <1 | <1 | <1 | <1 | <1 | 0.35 | 0.56 | 0.41 | <1 | 0.6 | 0.74 | <1 | 0.23 | 0.2 |
| Ba | 740 | 780 | 640 | 100 | 480 | 700 | 640 | 700 | 620 | 124 | 380 | <500 | 510 | 670 | <600 | 327 | 620 |
| La | 18.6 | 17.7 | 20.7 | 15.5 | 20.4 | 18.8 | 19.7 | 15.2 | 19.5 | 18.8 | 20.3 | 17.7 | 19.5 | 19.3 | 19.8 | 20.7 | 25.9 |
| Ce | 44 | 39.7 | 38.9 | 35 | 37 | 40 | 42.8 | 34.3 | 44.2 | 42 | 47 | 35 | 42 | 44.5 | 42 | 41.9 | 55.1 |
| Nd | <50 | 20.5 | <50 | <30 | <30 | <35 | 24.5 | 22 | 28 | 23 | 20 | 20 | 22 | 23 | 25 | 21.8 | 27.3 |
| Sm | 3.24 | 3.61 | 4.15 | 3.32 | 4.38 | 3.8 | 3.93 | 3.77 | 3.95 | 3.12 | 4.13 | 3.65 | 3.51 | 3.8 | 4.1 | 3.95 | 5.1 |
| Eu | 1.64 | 1.16 | 1.75 | 1.4 | 1.7 | 1.5 | 1.25 | 1.78 | 1.38 | 0.97 | 1.54 | 1.25 | 1.31 | 1.53 | 1.2 | 1.2 | 1.43 |
| Gd | 3.2 | <4 | 4.1 | 2.7 | <5 | <5 | 4.1 | 3.8 | 4.2 | 4.1 | 4.8 | 4.2 | 3.8 | 3.5 | 3.5 | 3.34 | 4.4 |
| Tb | 0.71 | 0.6 | 0.58 | 0.3 | 0.56 | 0.59 | 0.7 | 0.7 | 0.5 | 0.6 | 0.6 | 0.6 | <1 | <1 | 0.35 | 0.56 | 0.74 |
| Yb | 2.2 | 2.36 | 2.54 | 1.8 | 2.19 | 2.15 | 2.41 | 2.08 | 2.17 | 2.72 | 1.7 | 2.5 | 1.61 | 2.2 | 1.31 | 1.79 | 2.07 |
| Lu | 0.3 | 0.5 | 0.5 | <1 | 0.5 | 0.61 | 0.57 | 0.45 | 0.67 | 0.63 | 0.4 | 0.6 | 0.4 | 0.5 | 0.27 | 0.24 | 0.31 |
| Hf | 3.45 | 4.02 | <5 | 6.7 | 4.27 | 4.5 | 3.89 | 3.13 | 4.13 | 3.56 | 5.25 | 6.15 | 4.1 | <5 | 2.88 | 3.38 | 4.28 |
| Ta | <2 | 0.7 | <2 | <1 | <1 | <1 | <1 | 0.4 | <1 | <1 | 0.44 | <1 | 0.4 | <1 | 0.53 | 0.34 | 0.42 |
| Th | 11.5 | 3.24 | 3.22 | <5 | 4.38 | 3.37 | 3.85 | 3.96 | 3.68 | 2.62 | 3.77 | 2.2 | 2.68 | 4.51 | 4.27 | 3.54 | 3.99 |
| U | 1.5 | 0.64 | <2 | <2 | 1.31 | <1 | <1 | <1 | <2 | <1 | <1 | <1 | <1 | <1 | 0.87 | 0.94 | 0.64 |

(Koeberl et al. 1997; Glass et al. 2004). Contents of MgO are slightly lower in the fallback glass, and of $Na_2O$ slightly higher than in Ivory Coast tektites, but the variations are within factors of 0.8 and 1.3, respectively. The abundance of CaO is markedly higher in the fallback glass than in the Ivory Coast tektites: the average CaO content in the glass from 117A1 is 2.54 wt%, as compared to 1.38 wt% in the tektites (Koeberl et al. 1997), and 1.22 wt% (4 microtektites; Koeberl et al. 1997) and 1.78 wt% (16 microtektites; Glass et al. 2004). This results in enrichments by a factor of about 1.5–2 compared to Ivory Coast tektites.

The differences are also interesting in view of chemical compositions of target rocks and suevitic breccias at Bosumtwi (cf. Koeberl et al. 1998; Ferrière et al. 2007; Coney et al. 2007). Of the metasedimentary target rocks at Bosumtwi, only phyllites/shales/slates have CaO contents similar to those of the tektites; the overall average is more similar to the composition of the fallback glasses. Curiously, the average CaO content of fallback suevite (Ferrière et al. 2007) is higher (similar to those of the glasses) than that of fallout suevite (Boamah and Koeberl 2003), which is more similar to that of the distal ejecta (tektites and microtektites) (Table 7). It might be possible to extend the speculation mentioned above—that the microtektites were subjected to higher temperatures than the fallback glasses—to the chemical composition, where removal of volatile phases was more efficient for the distal ejecta at higher temperatures. Nevertheless, the average composition of the fallback glasses (proximal ejecta) agrees fairly well with that of the distal ejecta, as is shown by the Harker diagrams in Fig. 13, where it is evident that only the CaO content is significantly different. Good agreement exists also with the average target rock and suevitic breccia compositions at Bosumtwi (Table 7).

It is interesting to note that the chondrite-normalized platinum group element (PGE) abundance pattern of a (bulk) subsample of 117A1 is different from the patterns of target rocks and suevites outside the crater (Dai et al. 2005) and within the LB-07A and LB-08A drill cores (Goderis et al. 2007). This observation could indicate the presence of a small meteoritic component in the fallback layer (as noted by Goderis et al. 2007). However, such a component cannot be very large, because the total PGE content of the 117 samples, as especially noted for Ir, is not significantly higher than that of other Bosumtwi impactite samples.

## SUMMARY AND CONCLUSIONS

A microbreccia containing accretionary lapilli, mineral and lithic clasts including shocked quartz, as well as microtektite-like glass spherules and glass fragments of compositions similar to Ivory Coast tektites, was found in a core from borehole LB-05B in Lake Bosumtwi at the interface between impact breccias and post-impact lake

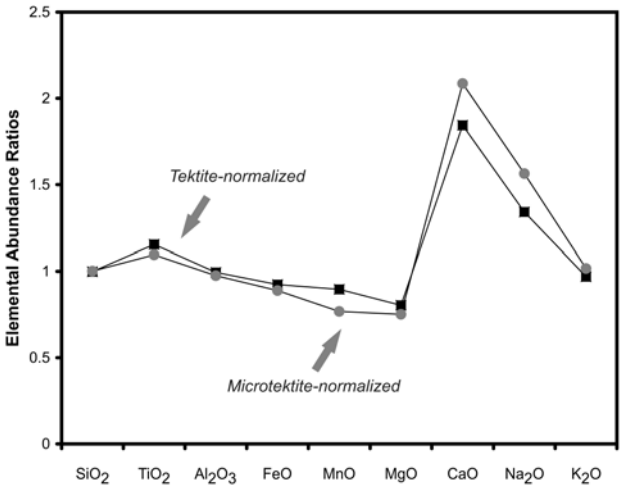


Fig. 12. The ratio of overall average (95 analyses) of glass fragments and glass spherules in fallback layer sample 117A1 versus average compositions of Ivory Coast tektites and microtektites (data from Koeberl et al. 1997) (Table 5). The glasses in the fallback layer have markedly higher contents of Ca, somewhat higher contents for Na, slightly higher contents of Ti, and slightly lower contents of Fe, Mg, and Mn, compared with both tektites and microtektites.

sediment at Bosumtwi. This material represents a layer of the last fine-grained fallback deposit. Glasses, as fragments and splash forms (e.g., spherules, teardrops, and dumbbells), make up the majority of the >125 μm size fraction in the top of the fallback layer. The fallback layer is graded in terms of grain size over the about 30 cm length of core studied here, from fine-grained in the top part (which is rich in shocked quartz and glass) and relatively coarser-grained towards the bottom of the section.

Shocked minerals, particularly quartz and K-feldspar, are also common at or near the top of the layer, but both their abundance and the shock degree recorded by them decrease with depth within a few tens of centimeters. The chemical composition of these glasses is very similar (with factors of less than 1.5 for most elements) to the compositions of Ivory Coast tektites and microtektites, with exception of the CaO content, which is higher by a factor of 2. However, the difference is less compared to fallback suevites (within the crater), which also have higher Ca contents that the fallout suevites (outside the crater). It appears that the distal ejecta (tektites and microtektites) experienced somewhat higher temperatures of formation than the proximal ejecta.

The whole fallback layer was deposited after the formation of the crater, including the immediate post-impact modification phase, was completed and all breccia had already filled the crater. Although numerical simulation of the Bosumtwi crater formation (Artemieva et al. 2004) did not involve the entire duration of cratering, to the end of the modification stage, it can be assumed that the fallback layer was deposited within hours after the impact. This agrees with considerations of atmospheric settling of particles larger than

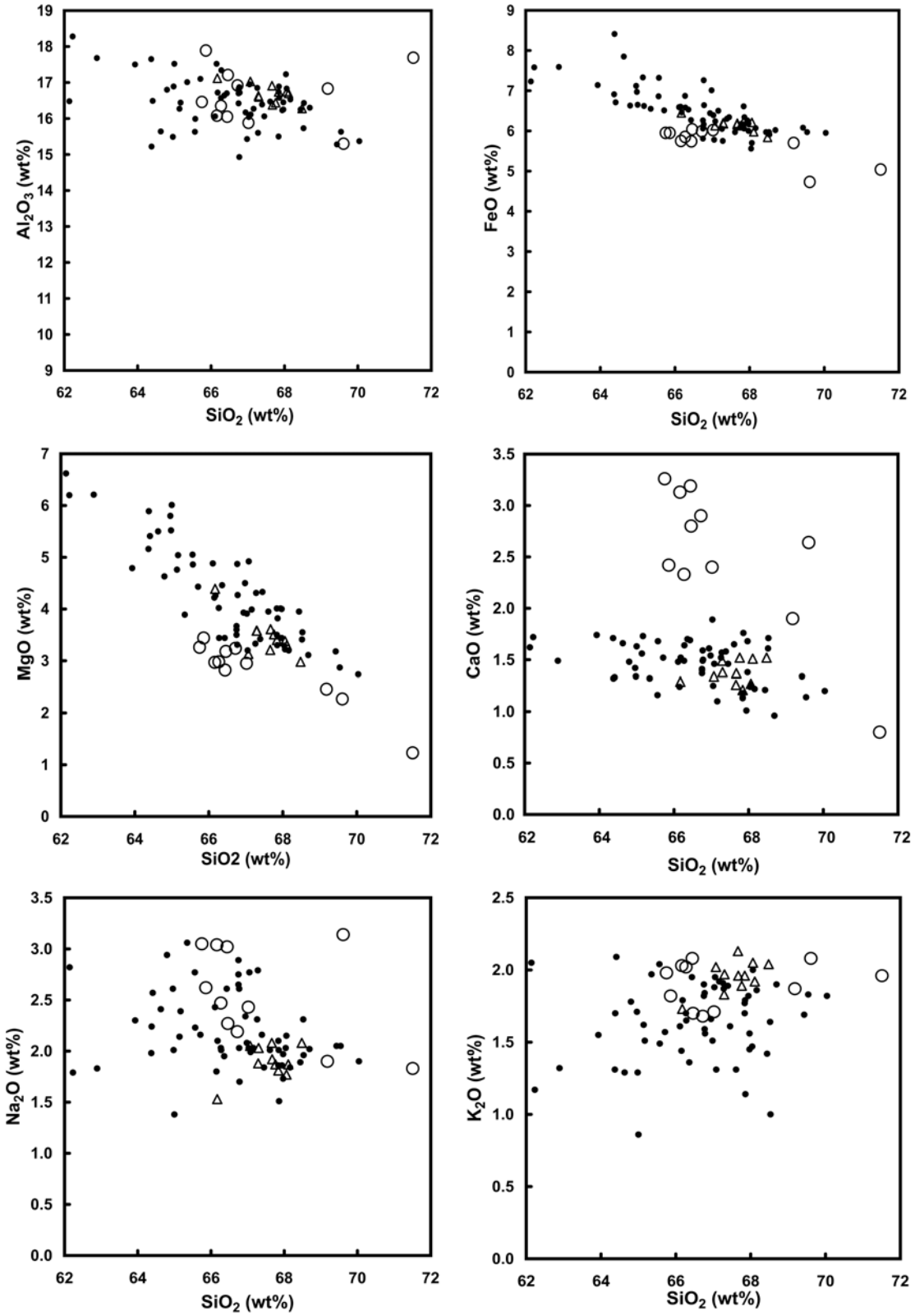


Fig. 13. Harker diagrams of major oxide contents in the glasses from the fallback layer in core BL-5B (this work) compared with data for Ivory Coast tektites (Koeberl et al. 1997) and Ivory Coast microtektites (Koeberl et al. 1997; Glass et al. 2004). The plots indicate the similarity in composition for most major elements except for CaO.

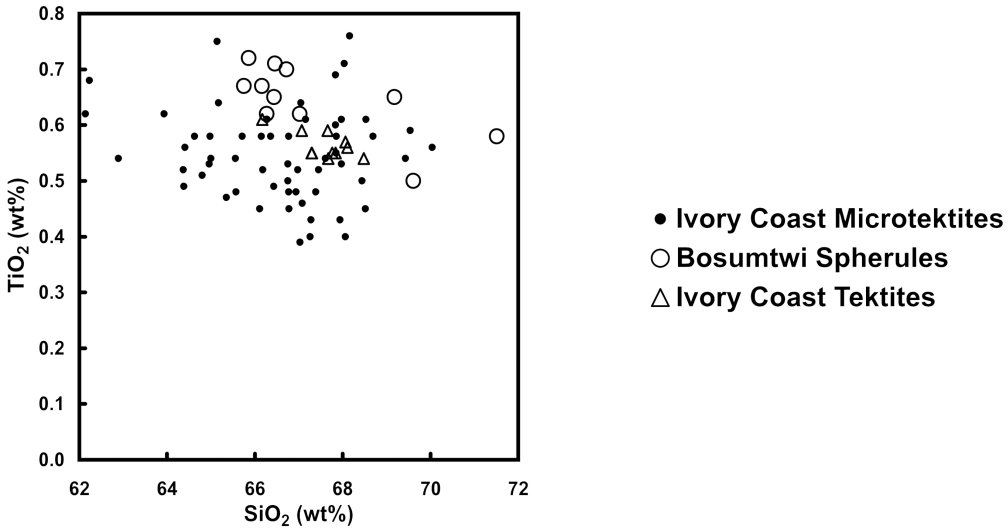


Fig. 13. *Continued.* Harker diagrams of major oxide contents in the glasses from the fallback layer in core BL-5B (this work) compared with data for Ivory Coast tektites (Koeberl et al. 1997) and Ivory Coast microtektites (Koeberl et al. 1997; Glass et al. 2004). The plots indicate the similarity in composition for most major elements except for CaO.

Table 7. Major-element composition of Ivory Coast tektites and microtektites (from Koeberl et al. 1997) compared with averaged compositions of the analyses of glass fragments and spherules from fallback layer sample 117-A1. All data in wt%.

| | Tektites[a] *n* = 11 | Microtektites[a] *n* = 4 | Microtektites[b] *n* = 16 | Glass 117A1 average A–F[c] *n* = 95 | Fallback suevite[d] *n* = 20 | Fallout suevite[e] *n* = 11 |
|---|---|---|---|---|---|---|
| $SiO_2$ | 67.58 | 67.37 | 66.4 | 67.47 | 63.16 | 63.58 |
| $TiO_2$ | 0.56 | 0.59 | 0.55 | 0.65 | 0.55 | 0.64 |
| $Al_2O_3$ | 16.74 | 17.07 | 16.9 | 16.64 | 14.65 | 15.58 |
| FeO | 6.16 | 6.40 | 6.65 | 5.69 | 5.49 | 6.58 |
| MnO | 0.06 | 0.07 | 0.07 | 0.05 | 0.06 | 0.11 |
| MgO | 3.46 | 3.70 | 4.27 | 2.78 | 2.50 | 1.43 |
| CaO | 1.38 | 1.22 | 1.73 | 2.54 | 2.67 | 1.39 |
| $Na_2O$ | 1.9 | 1.63 | 1.92 | 2.55 | 2.94 | 1.73 |
| $K_2O$ | 1.95 | 1.86 | 1.60 | 1.89 | 1.67 | 1.27 |
| Total | 99.79 | 99.91 | 100.09 | 100.26 | 99.70 | 100.01 |

[a]Koeberl et al. (1997).
[b]Glass et al. (2004).
[c]This work, average of 95 individual electron microprobe analyses along 10 of the profiles given in Table 5 and shown in Fig. 9 (averages of all unaltered glasses reported as "Avg" in Table 5: profiles A1, A2, B1, B2, C1, C2, D1, D2, F1, and F2).
[d]Ferrière et al. (2007); total includes 5.25 wt% loss on ignition.
[e]Boamah and Koeberl (2003); total includes 7.68 wt% loss on ignition.

50 μm from heights of about 10 km (Bluth and Rose 2004). The small (or absent) meteoritic component in the fallback layer deposited directly into the crater agrees with the suggestion of an oblique impact (angle between about 30 to 45° from the horizontal), which has also been invoked to explain the asymmetric distribution of the tektites relative to the crater location (Artemieva et al. 2004).

Fine-grained fallback layers in impact structures are very rare and restricted to well-preserved impact structures that were buried after their formation (e.g., at Chesapeake Bay) (Poag 2002), or where the impactites within the crater depression are covered with post-impact sediments (as in this case). The presence of the uppermost fallback layer at Bosumtwi indicates that the fallback and breccia units within the crater are complete, which confirms that Bosumtwi is probably the youngest and best-preserved large complex impact structure on Earth.

*Acknowledgments*–Drilling at Bosumtwi was supported by the International Continental Scientific Drilling Program (ICDP), the U.S. NSF-Earth System History Program under grant no. ATM-0402010, Austrian FWF (project P17194-

N10), the Austrian Academy of Sciences, and by the Canadian NSERC. This work was supported by the Austrian FWF (P17194-N10 (to C. K.). We are grateful to M. Talbot (University of Bergen, Norway) and J. Peck (University of Akron, USA) for advice and images, and to J. Peck and, especially, J. King (University of Rhode Island, USA) for help with obtaining samples of the fallback layer from core LB-05B. Thanks also to P. Claeys (Free University of Brussels) for the information about the PGE content of a subsample of 117A1. We appreciate helpful reviews by H. Dypvik and P. Claeys, as well as editorial advice by B. Milkereit.

*Editorial Handling*—Dr. Bernd Milkereit

## REFERENCES

Artemieva N. A., Karp T., and Milkereit B. 2004. Investigating the Lake Bosumtwi impact structure: Insight from numerical modeling. *Geochemistry Geophysics Geosystems*, 5, doi: 10.1029/2004GC000733.

Boamah D. and Koeberl C. 2003. Geology and geochemistry of shallow drill cores from the Bosumtwi impact structure, Ghana. *Meteoritics & Planetary Science* 38:1137–1159.

Bluth G. J. S. and Rose W. I. 2004. Removal processes of volcanic ash particles from the atmosphere. Proceedings, 2nd International Conference on Volcanic Ash and Aviation Safety. Office of the Federal Coordinator for Meteorology (OFCM), Washington, D.C. pp. 51–54.

Coney L., Reimold W. U., Gibson R. L., and Koeberl C. 2007. Geochemistry of impactites and basement lithologies from ICDP borehole LB-07A, Bosumtwi impact structure, Ghana. *Meteoritics & Planetary Science* 42. This issue.

Dai X., Boamah D., Koeberl C., Reimold W. U., Irvine G., and McDonald I. 2005. Bosumtwi impact structure, Ghana: Geochemistry of impactites and target rocks, and search for a meteoritic component. *Meteoritics & Planetary Science* 40: 1493–1511.

Ferrière L., Koeberl C., Reimold W. U., and Mader D. 2007. Drill core LB-08A, Bosumtwi impact structure, Ghana: Geochemistry of fallback breccia and basement samples from the central uplift. *Meteoritics & Planetary Science* 42. This issue.

French B. M. 1998. *Traces of catastrophe: A handbook of shock-metamorphic effects in terrestrial meteorite impact structures*. LPI Contribution #954. Houston, Texas: Lunar and Planetary Institute. 120 p.

Gentner W., Lippolt H. J., and Müller O. 1964. Das Kalium-Argon-Alter des Bosumtwi Kraters in Ghana und die chemische Beschaffenheit seiner Gläser. *Zeitschrift für Naturforschung* 19A:150–153.

Glass B. P. 1968. Glassy objects (microtektites?) from deep-sea sediments near the Ivory Coast. *Science* 161:891–893.

Glass B. P. 1969. Chemical composition of Ivory Coast microtektites. *Geochimica et Cosmochimica Acta* 33:1135–1147.

Glass B. P. and Pizzuto J. E. 1994. Geographic variation in Australasian microtektite concentrations: Implications concerning the location and size of the source crater. *Journal of Geophysical Research* 99:19,075–19,081.

Glass B. P. and Zwart P. A. 1979. The Ivory Coast microtektite strewn field: New data. *Earth and Planetary Science Letters* 43:336–342.

Glass B. P., Swincki M. B., and Zwart P. A. 1979. Australasian, Ivory Coast, and North American tektite strewn field: Size, mass and correlation with geomagnetic reversals and other earth events. Proceedings, 10th Lunar and Planetary Science Conference. pp. 2535–2545.

Glass B. P., Kent D. V., Schneider D. A., and Tauxe L. 1991. Ivory Coast microtektite strewn field: Description and relation to the Jaramillo geomagnetic event. *Earth and Planetary Science Letters* 107:182–196.

Glass B. P., Huber H., and Koeberl C. 2004. Geochemistry of Cenozoic microtektites and clinopyroxene-bearing spherules. *Geochimica et Cosmochimica Acta* 68:3971–4006.

Goderis S., Tagle R., Schmitt R. T., Erzinger J., and Claeys Ph. 2007. Platinum group elements provide no indication of a meteoritic component in ICDP cores from the Bosumtwi crater, Ghana. *Meteoritics & Planetary Science* 42. This issue.

Huffman A. R. and Reimold W. U. 1996. Experimental constraints on shock-induced microstructures in naturally deformed silicates. *Tectonophysics* 256:165–217.

Jones W. B. 1985. Chemical analyses of Bosumtwi crater target rocks compared with the Ivory Coast tektites. *Geochimica et Cosmochimica Acta* 48:2569–2576.

Jones W. B., Bacon M., and Hastings D. A. 1981. The Lake Bosumtwi impact crater, Ghana. *Geological Society of America Bulletin* 92:342–349.

Karp T., Milkereit B., Janle P., Danuor S. K., Pohl J., Berckhemer H., and Scholz C. A. 2002. Seismic investigation of the Lake Bosumtwi impact crater: Preliminary results. *Planetary and Space Science* 50:735–743.

Koeberl C. 1993. Instrumental neutron activation analysis of geochemical and cosmochemical samples: A fast and proven method for small samples analysis. *Journal of Radioanalytical and Nuclear Chemistry* 168:47–60.

Koeberl C. 1994. Tektite origin by hypervelocity asteroidal or cometary impact: Target rocks, source craters, and mechanisms. In *Large impacts and planetary evolution*, edited by Dressler B. O., Grieve R. A. F., and Sharpton V. L. GSA Special Paper #293. Boulder, Colorado: Geological Society of America. pp. 133–151.

Koeberl C. and Reimold W. U. 2005. Bosumtwi impact crater, Ghana (West Africa): An updated and revised geological map, with explanations. *Jahrbuch der Geologischen Bundesanstalt, Wien* (*Yearbook of the Austrian Geological Survey*) 145:31–70 (+1 map, 1:50,000).

Koeberl C., Bottomley R. J., Glass B. P., and Storzer D. 1997. Geochemistry and age of Ivory Coast tektites and microtektites. *Geochimica et Cosmochimica Acta* 61:1745–1772.

Koeberl C., Reimold W. U., Blum J. D., and Chamberlain C. P. 1998. Petrology and geochemistry of target rocks from the Bosumtwi impact structure, Ghana, and comparison with Ivory Coast tektites. *Geochimica et Cosmochimica Acta* 62:2179–2196.

Koeberl C., Milkereit B., Overpeck J. T., Scholz C. A., Peck J., and King J. 2005. The 2004 ICDP Bosumtwi impact crater, Ghana, West Africa, drilling project: A first report (abstract #1830). 36th Lunar and Planetary Science Conference. CD-ROM.

Koeberl C., Milkereit B., Overpeck J. T., Scholz C. A., Reimold W. U., Amoako P. Y. O., Boamah D., Claeys P., Danuor S., Deutsch A., Hecky R. E., King J., Newsom H., Peck J., and Schmitt D. R. 2006. An international and multidisciplinary drilling project into a young complex impact structure: The 2004 ICDP Bosumtwi impact crater, Ghana, drilling project—An overview (abstract #1859). 37th Lunar and Planetary Science Conference. CD-ROM.

Koeberl C., Milkereit B., Overpeck J. T., Scholz C. A., Amoako P. Y. O., Boamah D., Danuor S., Karp T., Kueck J., Hecky R. E., King J. W., and Peck J. A. 2007. An international and multidisciplinary drilling project into a young complex impact structure: The 2004 ICDP Bosumtwi Crater Drilling Project—An overview. *Meteoritics & Planetary Science* 42. This issue.

Lacroix A. 1934. Sur la découverte de tectites à la Côte d'Ivoire. *Comptes Rendus Academie des Sciences, Paris* 199:1539–1542.

Lippolt H. J. and Wasserburg G. J. 1966. Rubidium-Strontium-Messungen an Gläsern vom Bosumtwi-Krater und an Elfenbeinküsten-Tektiten. *Zeitschrift für Naturforschung* 21A: 226–231.

Littler J., Fahey J. J., Dietz R. S., and Chao E. C. T. 1961. Coesite from the Lake Bosumtwi crater, Ashanti, Ghana. GSA Special Paper #68. Boulder, Colorado: Geological Society of America. 218 p.

Montanari A. and Koeberl C. 2000. *Impact stratigraphy: The Italian record*. Lecture Notes in Earth Sciences, vol. 93. Heidelberg: Springer-Verlag. 364 p.

Poag C. W. 2002. Synimpact-postimpact transition inside Chesapeake Bay crater. *Geology* 30:995–998.

Reimold W. U., Brandt D., and Koeberl C. 1998. Detailed structural analysis of the rim of a large, complex impact crater: Bosumtwi crater, Ghana. *Geology* 26:543–546.

Schnetzler C. C., Pinson W. H., and Hurley P. M. 1966. Rubidium-strontium age of the Bosumtwi crater area, Ghana, compared with the age of the Ivory Coast tektites. *Science* 151:817–819.

Schnetzler C. C., Philpotts J. A., and Thomas H. H. 1967. Rare earth and barium abundances in Ivory Coast tektites and rocks from the Bosumtwi crater area, Ghana. *Geochimica et Cosmochimica Acta* 31:1987–1993.

Scholz C. A., Karp T., Brooks K. M., Milkereit B., Amoako P. Y. O., and Arko J. A. 2002. Pronounced central uplift identified in the Bosumtwi impact structure, Ghana, using multichannel seismic reflection data. *Geology* 30:939–942.

Shaw H. F. and Wasserburg G. J. 1982. Age and provenance of the target materials for tektites and possible impactites as inferred from Sm-Nd and Rb-Sr systematics. *Earth and Planetary Science Letters* 60:155–177.

Storzer D. and Wagner G. A. 1977. Fission track dating of meteorite impacts. *Meteoritics* 12:368–369.

Stöffler D. and Langenhorst F. 1994. Shock metamorphism of quartz in nature and experiment: I. Basic observation and theory. *Meteoritics* 29:155–181.

Wagner R., Reimold W. U., and Brandt D. 2001. Bosumtwi impact crater, Ghana: A remote sensing investigation. In *Meteorite impacts in Precambrian shields*, edited by Plado J. and Pesonen L. J. Impact Studies, vol. 2. Heidelberg: Springer-Verlag. pp. 189–210.